

Analyzing trends in precipitation patterns using Hidden Markov model stochastic weather generators

Christopher Paciorek
Department of Statistics, UC Berkeley

July 19, 2022

Abstract

We develop a flexible spline-based Bayesian hidden Markov model stochastic weather generator to statistically model daily precipitation over time by season at individual locations. The model naturally accounts for missing data (considered missing at random), avoiding potential sensitivity from systematic missingness patterns or from using arbitrary cutoffs to deal with missingness when computing metrics on daily precipitation data. The fitted model can then be used for inference about trends in arbitrary measures of precipitation behavior, either by multiple imputation of the missing data followed by frequentist analysis or by simulation from the Bayesian posterior predictive distribution. We show that the model fits the data well, including a variety of multi-day characteristics, indicating fidelity to the autocorrelation structure of the data. Using three stations from the western United States, we develop case studies in which we assess trends in various aspects of precipitation (such as dry spell length and precipitation intensity), finding only limited evidence of trends in certain seasons based on the use of Sen's slope as a nonparametric measure of trend. In future work, we plan to apply the method to the complete set of GHCN stations in selected regions to systematically assess the evidence for trends.

1 Introduction

Changes in precipitation are a critical component of potential impacts from climate change, via a variety of specific mechanisms, including flooding, drought, agricultural productivity, and effects on natural ecosystems (Lall et al., 2017; IPCC, 2022). Much research has focused on assessing the evidence for trends in overall precipitation and in extreme precipitation (Easterling et al., 2017; IPCC, 2021), sometimes using statistical extreme value analysis when focusing on very extreme precipitation (e.g., Westra et al., 2013; Risser et al., 2019). There is also an emphasis on formal "detection and attribution" analyses in the climate science literature, which attempt to lend statistical robustness to statements about the causal relationship of climate forcing variables (in particular greenhouse gases) with precipitation (e.g., Zhang et al., 2007). Another thread in the literature focuses on attributing individual extreme events, many of which are at least partly focused on precipitation (National Academies of Sciences, Engineering, and Medicine, 2016).

While extreme individual events (often daily extremes) are of course critically important, many questions about impacts and the fundamental climate science for understanding the mechanisms of changes relate to the entire pattern of precipitation, over the course of multiple days or much longer time periods. For such analyses, standard extreme value analyses are not as relevant or provide limited information because of limited data availability inherent in using time periods longer than a day. For example, the near-failure of the Oroville Dam in California occurred during a winter with high overall precipitation but for which no individual days or even events were particularly extreme (O'Brien et al., in prep.). As a second example, a critical question for agriculture is whether the frequency of droughts is changing with climate change. Zhang et al. (2021) report trends in mean dry interval length potentially indicative of increasing drought in the southwestern United States. More generally, a primary hypothesis about the impact of global warming on precipitation is one of intensification of dry and wet events, as a warming atmosphere is able to hold more water (Zhang, Furtado, Wu, Zhou, Chadwick, Marzin, Rostron, and Sexton, 2021)

In light of this, there is a need for statistical methods that go beyond analysing aggregate measures such as means or extremes (either annual or seasonal). One can develop metrics for phenomena of interest, such as the mean dry spell length (DSL) metric used in Zhang et al. (2021) and various metrics considered in O'Brien et al. (in prep.), and then carry out statistical analysis of trends on the metrics, but this has several shortcomings. First, one runs into multiple testing issues if considering multiple metrics, which will almost always be the case given the arbitrariness of any metric and the need for sensitivity analyses. Second, the use of complementary metrics to characterize the system (e.g., mean dry spell length and mean precipitation during wet events) may be of interest, and again multiple testing considerations would come into play. Perhaps most importantly, many of the metrics of interest cannot be computed in the face of missing data, which are common in observational data products. For example, one cannot compute the length of a dry interval in the face of a missing observation, with no real alternative to handle this apart from throwing out data (potentially entire seasons or years) contaminated by missingness. This is much more concerning than when computing mean precipitation, where an assumption that the missingness is non-informative can allow one to still compute a usable summary statistic. This missingness leads to omission of usable data (e.g., from years with only some data) and inability to assess trends further back in time as missingness becomes more common. This work seeks to develop a statistical method that can be used in this situation and to assess whether interesting trends in precipitation patterns can be detected from individual stations in light of the known low signal-to-noise ratio in

station-level precipitation data (Chandler et al., 2014; Easterling et al., 2017) (and see references in Risser et al., 2019).

We propose to use statistical models fit to daily data to characterize the patterns of precipitation and trends over time within a single model that can then be used for self-consistent inference about any metric of interest. The approach considers a metric to be a summary statistic functional of the joint distribution (over days) of precipitation, where the joint distribution accounts for the underlying temporal dependence structure of precipitation. Stochastic weather generators (SWGs) aim to account for the complicated temporal dependence of precipitation and hold promise for this sort of analysis, but the use of SWGs has focused on just that, serving to generate realistic weather time series (Wilks and Wilby, 1999), including for downscaling, rather than for carrying out inference about temporal changes. Various forms of SWGs have been proposed (see summaries in Chandler et al., 2014 and Ailliot et al., 2015), including hidden Markov models (HMMs) (e.g., Holsclaw et al., 2017; Stoner and Economou, 2020, among many others), generalized linear models (GLMs) (e.g., Chandler and Wheeler, 2002; Yang et al., 2005), and regional climate models. This work uses HMMs to characterize daily precipitation patterns, building in spline-based functions to account longer-term trends, including potential effects of climate change as well as modes of internal variability. The approach naturally handles missing observations via the usual HMM forward algorithm, with simple imputation of missing values using standard statistical methods.

We fit our HMM-based SWG using a Bayesian approach and use the fitted model as a statistical model to assess potential trends in two ways. First, we treat the problem as a missing data problem amenable to multiple imputation-based frequentist analysis. We make multiple imputations of the missing precipitation values using the fitted HMM and then use simple analyses of trend in any metric of interest, accounting for the imputation uncertainty. Second, we treat the problem in a fully Bayesian fashion, using the posterior of the fitted HMM to generate from the posterior predictive distribution of the metric of interest by simulating many time series of precipitation. The former has the advantage of relying on the data as much as possible and the model only for imputation, while the latter has the advantage of giving coherent posterior inference for any quantities of interest. Via either approach, we can then carry out trend analysis (e.g., using Sen’s slope (Sen, 1968) or linear regression) to estimate trends with uncertainty. We regard these trend estimates as useful first-order summaries of temporal variation, rather than believing that trends truly are monotonic or linear, in the spirit of Woody et al. (2021).

The modeling approach is purely empirical in that it doesn’t rely on extra information (such as other datasets, reanalysis, or even observations of quantities other than precipitation). This is beneficial for focused empirical work that seeks to report the evidence for trends based only on observations, and disadvantageous for other purposes as it leverages limited information and does not take account of the larger weather context about which much is known, particularly more recently in time with the availability of satellite data. The fitted model could also be used as a stochastic weather generator, though because it is unconnected to any forcing variables (i.e., covariates) and fit at individual locations, it has limitations in terms of when it would be appropriate to use.

We apply the methodology to several case studies related to specific scientific questions about potential trends in precipitation patterns, using data from the Global Historical Climatology Network (GHCN), which have been processed using various quality assurance checks (Menne et al., 2012). We consider potential trends over the periods 1920-2021, 1950-2021, and 1980-2021 out of scientific interest in trends over intervals of varying length, as well as diminishing data prior to

the 1920s, although we fit the HMM for 1900-2021 to include a boundary period.

The first case study is of drought in the southwestern U.S., motivated by the analysis of Zhang et al. (2021). We chose a station with nearly complete data in Winslow, Arizona (AZ) that was also used in Zhang et al. (2021). For this station, we focus on mean dry spell length (DSL) in each of the four standard seasons (DJF, MAM, JJA, SON), as a metric of meteorological drought. We also consider precipitation intensity, defined as the mean precipitation on days with precipitation.

The second case study is of prolonged dry spells and precipitation variability in California during the wet season (roughly October through April). For this we chose a station with nearly complete data in Berkeley, California (CA), focusing on mean dry spell length and precipitation intensity for each of three seasons (DJF, MAM, and SON, omitting JJA as essentially no precipitation falls in the area during the summer months). In recent years, California has experienced serious drought conditions, interspersed with wet years (Wang et al., 2017; Swain et al., 2018). In some of these years, there have been long periods during the wet season without precipitation, associated with a persistent high pressure system in the Pacific Ocean that blocks precipitation events (such as atmospheric rivers) (Wang et al., 2014; Swain et al., 2018), including a very long dry spell this past winter during January to March 2022. Our analysis focuses on assessing the evidence for trends in dry spell length and precipitation intensity as measures of such blocking behavior and the possibility of more pronounced precipitation variability expected with climate change (Wood et al., 2021).

The third case study is of precipitation patterns in the mountains of California, focused on the Feather River basin northeast of Sacramento. In the 2017 wet season, the Oroville Dam, a large dam that captures the flow of the Feather River, was severely damaged (Kasler and Hecht, 2017) because of high precipitation over a period of weeks. For this analysis we chose a station centrally located in the basin and with a nearly complete record in Quincy California. O’Brien et al. (in prep.) concluded that while no individual precipitation events were particularly extreme, there was a collection of many moderately-intense events during the time preceding the damage to the dam. Following O’Brien, our analysis focuses on assessing evidence for trend in the number of events, the average precipitation during the events, and maximum 40-day precip (a metric suggested in Swain et al. (2018) in part because of the historic 1861-1862 Sacramento flooding associated with extremely high precipitation over a similarly-lengthy time period). Given the hydrologic context, for this case study, we consider the full wet season defined as November through April.

In Section 2 we describe the Bayesian HMM and MCMC fitting approach, as well as our approach to model selection and assessment. In Section 3, we assess the fitted model and then apply the methodology to the three case studies.

2 Methods

Our model is an extension of the HMM developed by Stoner and Economou (2020) to model hourly precipitation. We modify the model to use with daily precipitation data, with flexible spline-based terms to capture variation over days within a season (*seasonal* terms) and variation over years (*yearly* terms). We fit the model separately for each season (generally DJF, MAM, JJA, SON), as the atmospheric drivers of precipitation vary widely over the course of a year (e.g., frontal systems in winter and convective systems in summer), and we have no reason to expect any time trends to be similar across seasons, related to both dynamics and thermodynamics. This approach allows

for there to be different long-term trends for different seasons without requiring specification of a complicated season-year interaction (discussed further below).

2.1 Hidden Markov model specification

As in Stoner and Economou (2020), our primary model uses three clone dry states and two wet states. The clone dry states allow for realistic multi-day dry spells, which would not be captured by a single dry state with a geometrically distributed number of days spent in the state (Stoner and Economou, 2020). The term *clone* reflects that all three of the dry states have the same conditional distribution for rainfall. Transitions between the dry states are not allowed, producing a mixture of geometric distributions for the time spent in the dry states. For the distribution over states on the first day of a season within each year, we use a Dirichlet distribution. For simplicity this distribution is assumed to not change over time.

2.1.1 Transition probabilities

The elements of the HMM state transition matrix for the five states are determined by $p_{jh} = Pr(z_{st} = h | z_{s-1,t} = j)$ for $h, j \in \{1, 2, 3, 4, 5\}$, where s indexes the day within a season and t indexes year, and where the two wet states are $h \in \{4, 5\}$. The full matrix, $P = \{p_{jh}\}$, is

$$\begin{pmatrix} p_{D_1} & 0 & 0 & q_1 & * \\ 0 & p_{D_2} & 0 & q_2 & * \\ 0 & 0 & p_{D_3} & q_3 & * \\ u_{11} & u_{12} & * & p_{W_1} & r_{12} \\ u_{21} & u_{22} & * & r_{21} & p_{W_2} \end{pmatrix},$$

where * indicates a entry computed such that each row sums to 1 and

$$\begin{aligned} q_1 &= (1 - p_{D_1})p_{DW_1} \\ q_2 &= (1 - p_{D_2})p_{DW_1} \\ q_3 &= (1 - p_{D_3})p_{DW_1} \\ r_{12} &= (1 - p_{W_1})p_{W_{12}} \\ r_{21} &= (1 - p_{W_2})p_{W_{21}} \\ u_{11} &= (1 - p_{W_1} - r_{12})p_{WD_1} \\ u_{21} &= (1 - p_{W_2} - r_{21})p_{WD_1} \\ u_{12} &= (1 - p_{W_1} - r_{12} - u_{11})p_{WD_2} \\ u_{22} &= (1 - p_{W_2} - r_{21} - u_{21})p_{WD_2}. \end{aligned}$$

Note that there are certain constraints built into the matrix, generally following Stoner and Economou (2020), to reduce the number of parameters, given this is already a flexible formulation with multiple dry and wet states. In particular, conditioning on the probability of transitioning from a dry state to a wet state, the probability of transitioning to a given wet state does not depend on the dry state being transitioned from. Similarly, conditioning on the transition from a wet state to a dry state, the probabilities of transitioning to a given clone dry state do not differ based on the wet state being transitioned from.

To account for variation in time, both long-term variation from internal variability and long-term trend potentially related to climate change, as well as variation over the course of a season, we use an additive representation with two spline terms for $\text{logit}(v)$ where

$$v \in \{p_{D_1}, p_{D_2}, p_{D_3}, p_{DW_1}, p_{W_1}, p_{W_2}, p_{W_{12}}, p_{W_{21}}, p_{WD_1}, p_{WD_2}\}:$$

$$\text{logit}(v_{st}) = \beta_0^v + X(s)\beta_s^v + X(t)\beta_t^v.$$

Consistent with the notion of clone states, the basis coefficients for the three dry states are taken to be equal: $\beta_s^{p_{D_1}} = \beta_s^{p_{D_2}} = \beta_s^{p_{D_3}}$ and $\beta_t^{p_{D_1}} = \beta_t^{p_{D_2}} = \beta_t^{p_{D_3}}$.

The basis matrices are computed using the *jagam* function from the *mgcv* package (Wood, 2017), using the default thin splate regression spline with a dimension of $K = 20$, chosen to be able to account for variation at the scale of weeks/months (seasonal terms) and decades (yearly terms), but not variability at the scale of individual days of the year or individual years. The splines are penalized in a Bayesian fashion using individual shrinkage priors (based on reparameterizing the splines using the *diagonalize=TRUE* argument in *jagam*):

$$\begin{aligned} \beta_{s,i}^v &\sim \mathcal{N}(0, \sigma_s^{2,v}), i = 1, \dots, K - 1 \\ \beta_{t,i}^v &\sim \mathcal{N}(0, \sigma_t^{2,v}), i = 1, \dots, K - 1 \end{aligned}$$

with noninformative priors for $\beta_{s,K}^v$ and $\beta_{t,K}^v$, which are associated with linear terms of season and year. For the variance parameters, we use flat priors on the standard deviation scale (Gelman 2006), specifically uniform on (0.001, 10) to prevent the MCMC from wandering in non-identifiable parts of the space for the variance components. For the intercept terms we use reasonably non-informative priors restricted to avoid placing heavy weight on extreme probabilities.

To avoid additional complexity from another spline term, we assume that the seasonal effect does not change across years. We consider this a first-order approximation, as changes in seasonality may well occur over many years, but we feel this is justified given the limited power seen in detecting changes in the main effect of year (Section 3.3).

2.1.2 Precipitation distribution

There has been extensive discussion in the climate science and statistics literature on appropriate distributions for precipitation. Furrer and Katz (2008) find that gamma distributions have too light a tail and cannot capture the right tail of the distribution accurately. Stoner and Economou (2020) use a generalized Pareto distribution (GPD) for non-zero precipitation in each HMM state, while Naveau et al. (2016) develop a generalization of the GPD. In contrast Martinez-Villalobos and Neelin (2019) argue for the use of gamma distribution. We considered using both the gamma distribution and the generalized Pareto distribution. Since we found the gamma distribution to perform best (Section 3.1), we next present that as the primary model.

The model uses a mixture of a point mass at zero and a gamma distribution for precipitation conditional on state, $p(R_{st}|z_{st})$. The three dry states are considered as a single state, with a single precipitation distribution, while each of the two wet states has their own precipitation distribution. Thus for each of these three distributions, $k \in \{1, 4, 5\}$, we have:

$$p(R_{st} = r_{st}|z_{st} = k) = \pi^k + (1 - \pi^k)Ga(\xi_{st}^k, \sigma_{st}^k),$$

where ξ is the shape parameter and σ the scale parameter. For the log of ξ_{st}^k and σ_{st}^k , we use the same spline representations of season and year as described above for the logit of the probabilities used to construct the HMM state transition matrix. The probability of no daily precipitation, π^k , is assumed not to vary over season or year, to help reduce non-identifiability from the HMM state transition probabilities trading off with the probability of precipitation given state. To help enforce that the dry state would generally have low precipitation, we assume there is no variation over season or year for the dry state ($\xi_{st}^1 = \xi^1$ and $\sigma_{st}^1 = \sigma^1$).

As an alternative model, we also considered the GPD in place of the gamma distribution above, as in Stoner and Economou (2020), with ξ_{st}^k and the log of σ_{st}^k being spline-based representations of season and year for the shape and (log) scale parameters of the GPD.

Rounding The GHCN data are rounded to the nearest .01 inch. To account for this, we create a likelihood for the discretely-observed values by integrating the underlying gamma distribution (or GPD) over plus or minus .005 inches of the reported value. That said, the degree of rounding is not so discretized that one would necessarily expect that the usual assumption of continuous values would pose a problem. For some stations (e.g., Quincy, CA but not Berkeley, CA), there appears to be some additional rounding to the nearest 0.1 inches or (in some cases 0.05 inches) for some of the values, with more such apparent rounding in earlier years. We do not account for the rounding to coarser increments as this would necessitate modeling to account for the unknown fraction of observations rounded to different degrees.

2.1.3 Identifiability

Models with unknown states, such as HMMs, are prone to identifiability issues, which can affect MCMC convergence and mixing. While we are not able to completely avoid this, we impose some constraints to reduce the problem, in addition to the already-specified constraints built into the model. Specifically, to enforce the meaning of dry versus wet states, we constrain $\pi^1 > \pi^4 > \pi^5$, and we enforce that the mean of the gamma distribution (or median of the GPD) are increasing over the states (from dry to wet state 1 to wet state 2) separately for every season-year value during the MCMC fitting. We also constrain $p_{st}^{WD1} > 0.4$ and $p_{st}^{WD2} > 0.4$ for each value of s and t to encourage that the first dry state be entered most frequently and the third dry state least frequently. Finally, in early runs, we found that the parameters of the second wet state could wander off into parts of the parameter space unconstrained by the data and produce unrealistically large precipitation values when simulating from the posterior predictive distribution (simulating precipitation in the thousands or even millions of cm), generally when the probability of entering the second wet state was low (e.g., during seasons that are generally dry in a given location). To avoid this, we constrain the mean of the gamma distribution (or median of the GPD) at every season-year time point to be less than the maximum daily precipitation over all years for a given location-season.

In our MCMC assessments, we examined trace plots and generally found reasonable mixing for the individual parameters in the model, but with some indications of non-identifiability, for example with the shape and scale parameters of the gamma distributions for the two wet states transitioning between different levels that correspond to changes in some of the probabilities in the transition matrix. This is not surprising given the multiple dry (clone) and wet states of the

HMM. Given the inherent non-identifiability, we focused assessment of mixing on various summary statistics of the posterior predictive distributions (Section 2.2).

2.1.4 Seasonal modeling

Our initial model attempted to represent all four seasons in a single model. It used three spline terms to capture temporal trends across day of season, year, and the interaction of the two. This required careful consideration of the spline basis terms to avoid strong posterior correlations (Wood, 2017), and even with this, we found that MCMC mixing was rather worse than the single-season models. For simplicity, we chose to stratify by season as discussed above, rather than proceeding with the full season-year model. However, we note that the mixing difficulties revealed themselves in terms of non-identifiability given the multiple dry and wet states, as discussed above, and if one focuses on posterior predictive quantities reflecting the model’s characterization of the observable precipitation patterns, the full model might be worth further consideration.

2.2 Fitting

For Bayesian estimation using Markov chain Monte Carlo (MCMC), one can choose whether to estimate latent states or to integrate over them, using a variety of techniques. For HMMs, the integration is straightforward using the standard forward algorithm, which we use. We assume missing data as having their missingness unrelated to the unknown value, but of course related to the time point (day of season and year), so considered to be missing at random (MAR), accounted for by the season and year spline terms.

We use NIMBLE version 0.12.2 (de Valpine et al., 2017; NIMBLE Development Team, 2022) to carry out the MCMC, implementing the forward algorithm as a user-defined function. The bulk of the computation in the MCMC involves calculation of the precipitation density for each observation given each potential state and the forward algorithm computations. We also note that the discretized likelihood incurs the cost of multiple gamma CDF calculations, which are costly. We are careful to only recalculate the density values for each observation under each potential state when the parameters of the precipitation distribution (and not the parameters of the transition matrix) change. For missing values, we impute precipitation using the forward filtering backward sampling (FFBS) algorithm, implemented as a user-defined sampler in NIMBLE. This imputes from the full posterior distribution for the states at all times and then draws from the precipitation distribution given the imputed state. Note that one could draw from the forward algorithm’s probability distribution over the states, but this would ignore the information from the future that is relevant for prediction, although the impact of this would be lessened for longer strings of sequential missing values.

For each location-season of interest, we fit the model to all data in 1900-2021 (starting with winter of the year 1900, which includes months from 1899) and concluding with the fall season of 2021). We ran five MCMC chains of 20,000 iterations each (each chain taking about one day on a single CPU core), taking a conservative burn-in period of 5,000 iterations for each chain, and thinning by 10 to reduce storage and computation, producing a total of 7,500 posterior samples. We use NIMBLE’s adaptive Metropolis samplers for each scalar parameter. Initial exploration of other samplers (blocking, slice sampling, etc.) did not indicate better performance from other

approaches. For posterior predictive quantities, we simulated one full time series for each of the 7,500 posterior samples.

Given the aforementioned indications of non-identifiability, we focus on posterior predictive quantities from the model that characterize the climatology that the model produces for the period 1920-2021. These include

- several values of the precipitation CDF (greater than 3 mm, 10 mm, 20 mm) by year and by day of season;
- transition probabilities between dry and wet days (using a cutoff of 3 mm) by year;
- mean dry spell length and precipitation intensity by year; and
- Sen’s slope for dry spell length and precipitation intensity, as an aggregate summary.

Using posterior predictive time series simulations, we compute the \hat{R} and ESS as suggested in Vehtari et al. (2021) and available in the RStan R package version 2.21.2 (Stan Development Team, 2020). Given the large number of diagnostic quantities (e.g., one per year for each location-season pair in many cases), we report summaries of the distribution (over the various years or days of season) of these diagnostics for the various quantities for each of the eight location-season pairs of the case studies. Table 3 (Appendix) shows percentiles of \hat{R} for the eight location-seasons. In essentially all cases, mixing seems reasonable. Table 1 shows \hat{R} , ESS, and a measure of ESS focused on tail quantities (Vehtari et al., 2021) for Sen’s slope. In most cases, mixing seems reasonable, but for JJA for Winslow for mean dry spell length, there is indication of concern (and perhaps for DJF for Berkeley for both dry spell length and precipitation intensity and JJA for Winslow for precipitation intensity). This is somewhat surprising given the diagnostics for the yearly mean dry spell length and precipitation intensity (Table 3 (Appendix), columns 11-12) do not indicate any issues. It appears that Sen’s slope may be sensitive to very subtle changes in the yearly values that are present in the posterior samples, perhaps related to label-switching/non-identifiability of the HMM. Considering Sen’s slope over later periods (1950-2021 and 1980-2021), the \hat{R} values for mean dry spell length for JJA for Winslow are smaller (1.036 and 1.010). In future work, we plan to explore whether the use of Hamiltonian Monte Carlo improves upon the MCMC sampling strategy used here.

2.3 Model selection

We do not carry out extensive model selection, as we have constructed a flexible model that nests simpler models within it. The use of separate variances for the spline term coefficients, estimated as part of the fitting process, allows for shrinkage of the day-of-season- and year-varying effects for the various states, building in the ability for the fitting process to estimate simpler models when sufficient to fit the data well, as would be favored by the usual inherent Bayesian complexity penalty (Jefferys and Berger, 1992; MacKay, 2003). With regard to the number of states, if fewer states are needed, the fitting could estimate the transition probability into an unneeded state to be near zero, thus allowing the spline terms for that state to shrink to having no seasonal or yearly variation.

That said, we do carry out two types of model comparison for a subset of location-season pairs (DJF and JJA for Winslow, DJF for Berkeley, and November-April for Quincy,). First we compare

Table 1: MCMC diagnostics (\hat{R} and bulk ESS and tail ESS) for Sen’s slope (for 1920-2021) for mean dry spell length and precipitation intensity for the eight location-seasons.

	mean dry spell length			precipitation intensity		
	\hat{R}	ESS, bulk	ESS, tail	\hat{R}	ESS, bulk	ESS, tail
Winslow AZ, DJF	1.012	1114	3515	1.005	2545	6101
Winslow AZ, MAM	1.000	5982	5744	1.000	4978	6733
Winslow AZ, JJA	1.089	35	121	1.015	361	5750
Winslow AZ, SON	1.000	5075	6364	1.000	5410	6492
Berkeley CA, DJF	1.015	424	5746	1.024	184	1955
Berkeley CA, MAM	1.006	3605	6718	1.011	1351	5623
Berkeley CA, SON	1.000	6507	6928	1.001	5587	6768
Quincy, wet (Nov-Apr)	1.001	4694	6548	1.001	5115	7144

the gamma distribution and GPD for precipitation. Second, we compare the full model to a model with no yearly trend terms as a guard against overfitting. We use both a held-out test set and WAIC. For the assessment on the test set, we hold out individual years of data at a time (every tenth year for the years 1910 through 2020) and assess one-day ahead predictions and full-year predictions. I.e., the one-day ahead cross-validation calculates the likelihood of the held-out observation for a given day, with the prediction conditioned on all the data before that day (including the earlier held-out data). The full-year predictions condition only on the training data, using the forward algorithm to calculate the predictive distribution for each held-out observation. In addition, to compare the gamma and GPD-based models, we examine Q-Q plots, as a key distinction between these models is the right tail of the distribution.

Note that WAIC is a pointwise measure, so one must choose the unit of observation (Vehtari et al., 2017), and for temporal data, it is not clear that treating each day as an observation is appropriate any more than it would be for cross-validation. Instead we choose to treat each year as a multivariate observation, which is easily done when requesting WAIC calculation in NIMBLE (Hug and Paciorek, 2021). Also note that for logistical simplicity and to be able to compare held-out and WAIC results from the same model fits, we calculate WAIC in conjunction with the hold-out test set analysis, so the training data for WAIC are not the full dataset (i.e., every tenth year is excluded).

2.4 Model assessment

Given the a best model based on the model selection process, we assess the fit of the model by comparing summary statistics using the posterior predictive distribution, using the 7,500 simulated precipitation time series and masking the simulated series to match the missingness in the actual data (with one exception noted later). We consider the following summary statistics:

- total season precipitation as a function of year;
- probability of daily precipitation as a function, marginally, of year and season;
- precipitation intensity (mean precipitation on days with precipitation greater than 3 mm) as a function, marginally, of year and season;

- conditional distributions for (discretized) precipitation given (discretized) previous day precipitation as a function, marginally, of year and season;
- Q-Q plots for daily precipitation, three-day precipitation and ten-day precipitation over all years and seasons, where three- and ten-day precipitation are calculated using all possible (overlapping) moving blocks, thereby capturing the full precipitation of entire events; and
- mean dry spell length as a function of year, and Q-Q plots for dry spell length, where precipitation less than 3 mm is considered a dry day, and spells are truncated by the beginning and end of a season.

Some of these diagnostics target various marginal distributions and don't assess model performance relative to some of the multi-day phenomena of interest, while others directly address multi-day fidelity.

Note that imposing the same missingness pattern on the simulated values as is present in the actual data allows for comparison of the empirical and the simulated but also means that the diagnostic plots should not be interpreted as showing the within-season or yearly patterns directly because the data are not missing completely at random.

2.5 Trend analysis

We use an imputation-based frequentist analysis as well as a fully Bayesian approach to trend assessment. Given the widespread use of Sen's slope in climate science, we focus on that statistic here, but others (such as other forms of robust regression or simple linear regression) could be easily substituted. We consider three time periods: 1920-2021, 1950-2021, and 1980-2021.

2.5.1 Imputation-based analysis

We take a frequentist-based multiple imputation approach, using the 7,500 posterior imputations for the missing observations. For each imputation, we use the now-complete data to estimate Sen's slope. We then use Rubin's rules for combining the results (after a continuity correction (Helsel and Frans, 2006) applied to each Mann-Kendall S statistic), with the p-value computed using the z-statistic for the mean of the corrected S statistics.

2.5.2 Model-based analysis

We take a fully Bayesian predictive approach, using the 7,500 posterior predictive time series simulations. We consider trend estimates to be summary statistics, rather than parameters (or direct functionals of parameters) of the model, in the spirit of Woody et al. (2021). The fully Bayesian approach has the benefit, compared to the imputation-based approach, of providing a Bayesian joint posterior distribution over any functionals of interest. It has the downside of relying fully on the HMM posterior predictive distribution being an adequate representation of the aspects of precipitation affecting the metric of interest. While our diagnostics indicate good fits (Section 3.2), one may be cautious about trends in extremes, such as extreme daily values or multi-day events such as many-day precipitation or very long dry or wet spells, for which one might be concerned that a first-order HMM with gamma distributions for precipitation (even one with multiple states) might not be adequate.

2.6 Case studies

Our analysis focuses on three case studies: (1) drought in the southwestern United States using the Winslow AZ station; (2) winter (wet season) precipitation variability in California using the Berkeley CA station; and (3) winter (wet season) mountain precipitation events using the Quincy CA station. We use the GHCN data for these stations, omitting observations failing any quality assurance checks, and setting trace precipitation to zero.

For Winslow and Berkeley, we focus on mean dry spell length. Dry days are considered to be those with less than three mm precipitation, given evidence that such low amounts do not penetrate to the plant rooting zone (Huxman et al., 2004). We only consider days within the season, so dry spells at the beginning and end of the season are truncated. This simplification avoids having to make calculations with days outside the season, keeping the inference focused on precipitation patterns within the season, but with the caveat that the estimates do not reflect the true lengths of dry spells. Note that this induces a highly discrete distribution over mean DSL in seasons with few events, with the mean DSL with one precipitation event equalling ~ 45 and with two precipitation events ~ 30 . We also consider precipitation intensity, defined as the mean precipitation on days with precipitation, again defined based on the three mm cutoff.

For Quincy, given the Oroville Dam event and interest in precipitation events that led to the damage, we use metrics related to precipitation events, reflecting intensity and frequency of the events, in particular the number of wet spells in the wet season, mean precipitation of the wet spells, and maximum precipitation of any 40-day period in the season.

3 Results

3.1 Model comparison

For our selected location-season pairs, model selection based on held-out data and WAIC is equivocal with regard to using the gamma distribution versus GPD (Table 2). However, for certain GPD parameter values, the GPD can generate unrealistically high precipitation (values in the hundreds, thousands, and even higher), occurring when the shape parameter approaches one or greater. The result is that the GPD-based simulated values have an overly heavy far right tail. While Q-Q plots indicate that the overly heavy tail only affects extreme precipitation (e.g., approximately the largest 0.2% of values for Winslow AZ), it would raise the issue of what to do with these values in an analysis. The suitability of the gamma distribution even in the far right tail in light of results indicating that a gamma distribution cannot capture the heavy tail of precipitation (Furrer and Katz, 2008) likely relates in part to our mixture over multiple states, which provides more flexibility in capturing the underlying distribution. Another disadvantage of the GPD is that in some MCMC samples, the right tail is bounded for some season-year values (i.e., $\xi_{st} < 0$) and one can find a small number of held-out observations beyond the estimated bound and therefore deemed impossible by the fitted distribution, complicating model comparison. Given the similarity in the model comparison criteria and these disadvantages of the GPD, we choose to use the gamma model.

With regard to trend, there is not clear evidence in favor of or against the models with yearly trend in most cases, with the most evidence for trend in JJA in Winslow. While there is not strong evidence for overall trend, there is also little evidence that the full model is overfitting. In light of this, we proceed with the full model because doing so systematically allows us to avoid choosing

Table 2: Model comparison based on the negative log-likelihood (NLL) of hold-out data for one-day ahead prediction and full yearly prediction and WAIC (posterior standard deviation of the negative log-likelihoods and pWAIC in parentheses). Lower values indicate better fits.

		NLL, one-day	NLL, full-year	WAIC (pWAIC)
Winslow (DJF)	gamma, no yearly trend	926.1 (2.9)	941.6 (2.4)	14901 (53)
	gamma, yearly trend	930.9 (3.8)	943.5 (3.5)	14860 (86)
	GPD, yearly trend	926.5 (4.4)	942.7 (4.3)	14865 (55)
Winslow (JJA)	gamma, no yearly trend	1119.1 (2.5)	1142.4 (2.2)	21185 (61)
	gamma, yearly trend	1114.1 (3.3)	1137.2 (2.9)	21145 (88)
	GPD, yearly trend	1114.2 (4.0)	1137.7 (3.9)	21148 (74)
Berkeley (DJF)	gamma, no yearly trend	2323.9 (3.3)	2430.1 (3.6)	38284 (67)
	gamma, yearly trend	2329.3 (4.1)	2436.9 (5.2)	38321 (143)
	GPD, yearly trend	2331.3 (10.5)	2439.0 (11.7)	38299 (92)
Quincy, wet (Nov-Apr)	gamma, no yearly trend	3845.2 (2.6)	4037.6 (4.0)	76450 (60)
	gamma, yearly trend	3849.5 (3.8)	4038.5 (5.3)	76383 (116)
	GPD, yearly trend	3858.3 (20.6)	4050.0 (23.1)	76473 (110)

between models using what would necessarily be a somewhat arbitrary cutoff. The shrinkage possible in the full model protects against overfitting and detecting trends where there are none. As seen in our results, we find no evidence of trends in many cases, suggesting that overfitted trends are not a concern. An additional benefit of the full model is that the spline terms can account for low-frequency variability, such as induced by internal variability in the climate system (e.g., the recent multi-year drought in the western U.S.).

3.2 Model assessment

We next turn to assessing the fit of the chosen gamma model with yearly trend terms based on the posterior predictive distribution over simulated precipitation time series for the eight location-season pairs.

Fig. 1 shows quantile-quantile (Q-Q) plots comparing the simulated and observed daily, three-day, and ten-day precipitation. In general, the simulated distributions match the observed distributions very well, with the main exception being that simulated multi-day precipitation for MAM in Berkeley is too low for the most extreme events.

Fig. 2 shows the mean dry spell length (DSL) by year for the observed and simulated values. The simulated values match the observed values well, with simulation uncertainty intervals doing a reasonable job of covering the observations, albeit with the uncertainty intervals appearing to overcover the observed values.

Figs. 8-19 (Appendix) display various additional diagnostic plots, showing the observed values compared to the simulated values for total seasonal precipitation, probability of precipitation, precipitation intensity, probabilities of discretized precipitation given the previous day's discretized precipitation, and Q-Q plots for dry spell length. In general, the simulated values match the observed values well when accounting for stochasticity in the observed values. The simulation uncertainty intervals do a reasonable job of covering the observations, with some indications of over-

coverage, suggesting that the simulated values are a bit too variable. This is perhaps not surprising as the simulations are probabilistic, while the real data are generated by a physical system with embedded constraints.

3.3 Case studies

Fig. 3 shows the mean dry spell length and precipitation intensity by year for each of the eight location-season pairs, with imputation uncertainty. The plots suggest a low signal-to-noise ratio.

3.3.1 Arizona drought

Fig. 4 presents trend results for Winslow for DJF, MAM, JJA and SON. We see some evidence for trends in both dry spell length (increasing) and precipitation intensity (decreasing) for MAM and JJA for some of the time periods. One cautionary note is that MCMC mixing for JJA for the longer time periods is problematic (Table 1), although we don't expect this to have much impact on the imputation-based analysis given the negligible missing data for this time series.

3.3.2 California winter dry spells

Fig. 5 presents trend results for Berkeley for DJF, MAM, and SON. We omit JJA because of the extreme dry season during those months, with very little precipitation (e.g., see Fig. 10 where the probability of precipitation at the end of MAM and beginning of SON is very low). There is little evidence for trend over any of the three time periods for either metric, apart from an increase in precipitation intensity for DJF over 1920-2021. This suggests that, at least as measured by the dry spell length and precipitation intensity metrics, we do not see evidence in support of trend in blocking behavior or increased within-season variability of precipitation.

3.3.3 California mountain precipitation

Fig. 6 shows the number of wet spells, mean spell-level precipitation, and maximum 40-day precipitation for Quincy, with imputation uncertainty. The plots suggest a low signal-to-noise ratio.

Fig. 7 presents trend results for Quincy. There is little evidence for trend over any of the three time periods or three precipitation metrics. Thus we do not see evidence that the precipitation pattern resulting in the Oroville Dam event was related to a long-term trend in the pattern of precipitation events as measured by our metrics. Of course our metrics do not capture other potentially-relevant aspects of climate relevant to the event, such as rain-on-snow events that can cause a burst of snowmelt.

4 Discussion

We have presented a stochastic weather generator-based approach to inference for trends in daily precipitation patterns, focusing not on traditional short-term extremes but on multi-day and longer precipitation patterns that may have important impacts or reflect changing climate. The approach focuses on careful modeling of precipitation time series using hidden Markov models in a Bayesian

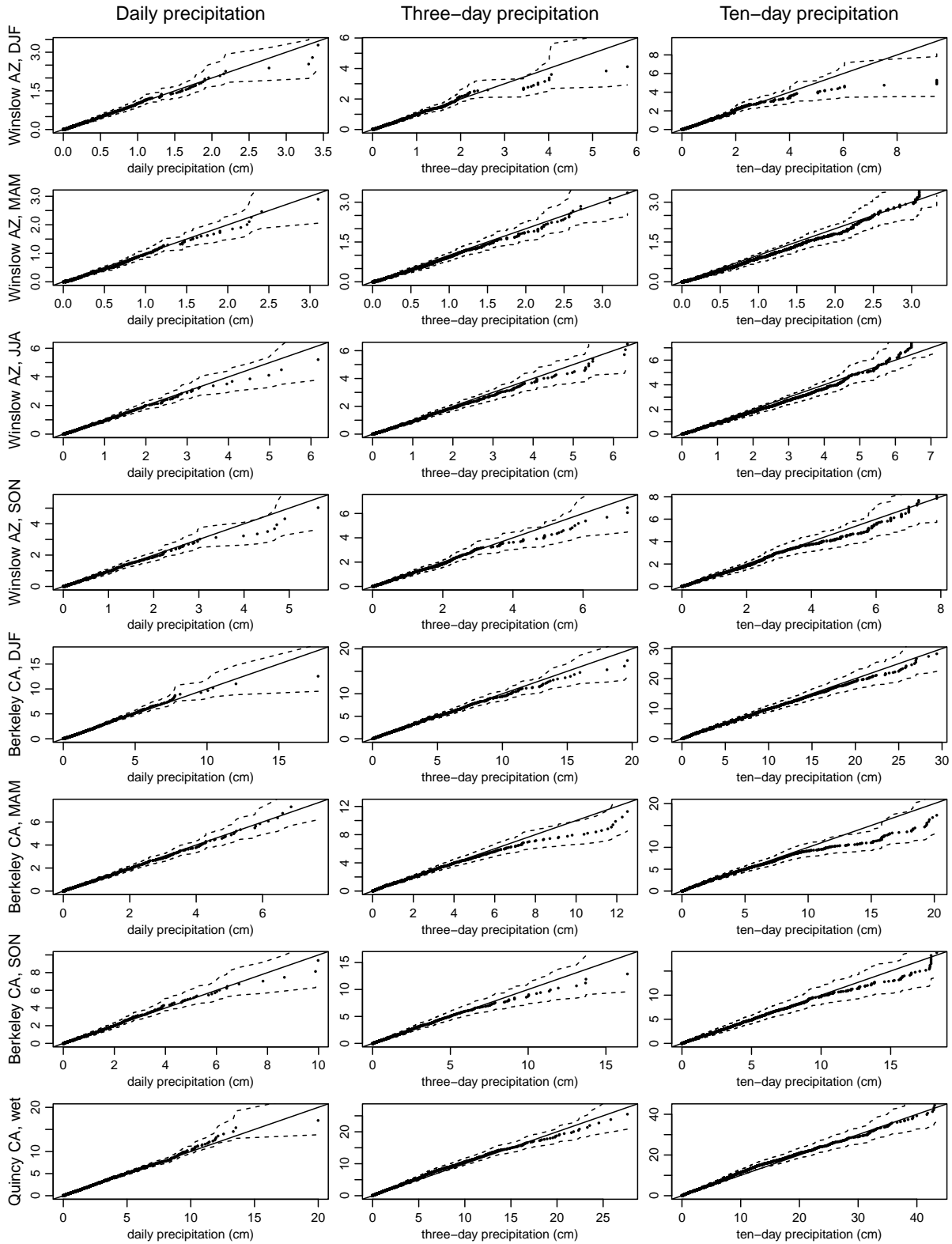


Figure 1: Median and 95% posterior predictive distribution intervals for Q-Q comparisons of the simulated versus observed daily (left column), three-day (middle), and ten-day (right) precipitation (cm) for the eight location-season pairs (rows). The median and 95% intervals are taken over Q-Q comparisons of each of the simulated time series against the observed values. If simulated values are consistent with the observed values, we expect the points (the median values) near the 1:1 line and the intervals to generally cover the 1:1 line.

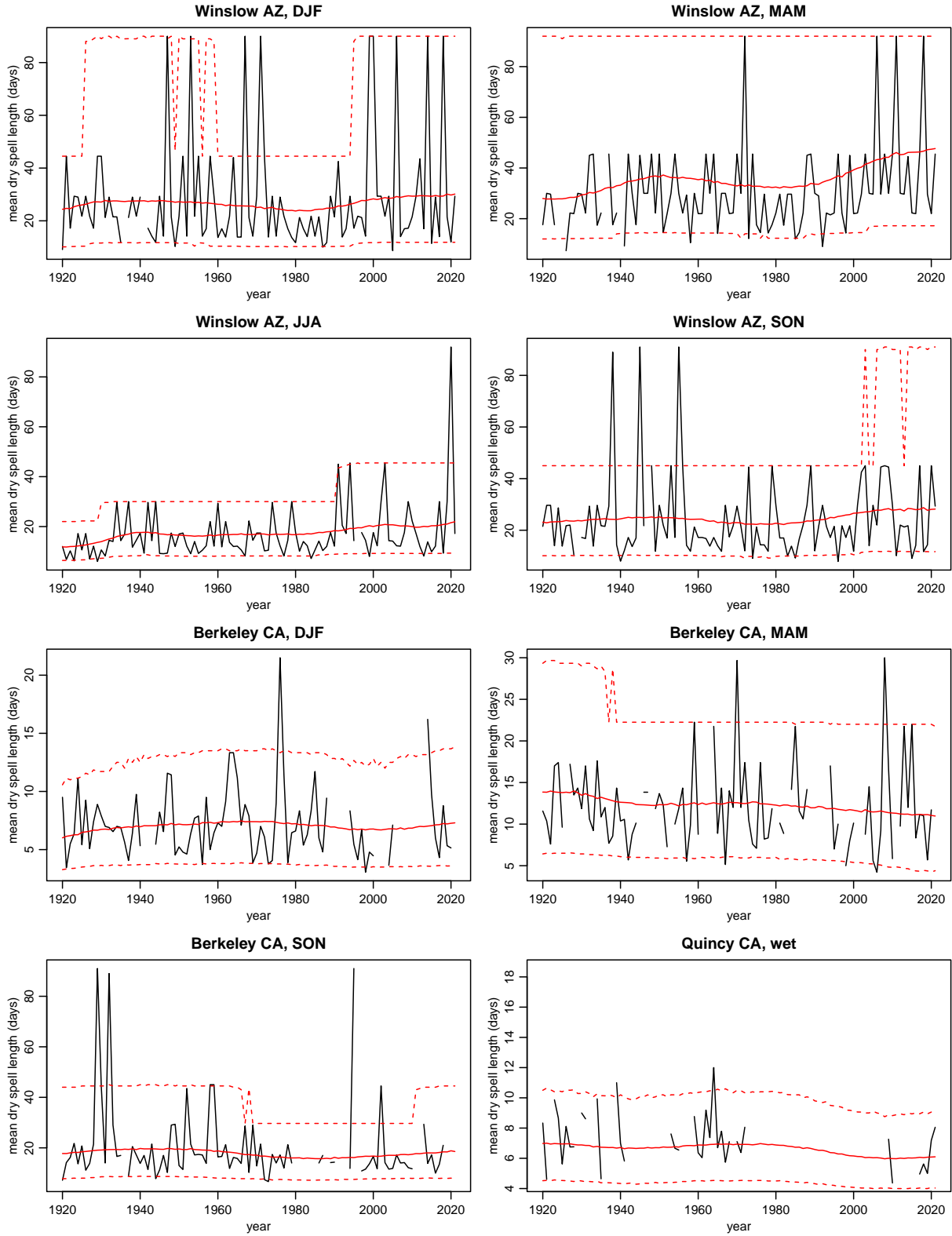


Figure 2: Observed (black) versus simulated (red) mean dry spell length by year for the eight location-season pairs, omitting observed values (but not simulated values, in order to show predicted temporal variation) for years with any missing days. Simulated values are the mean over the simulations, with 90% posterior predictive uncertainty bands.

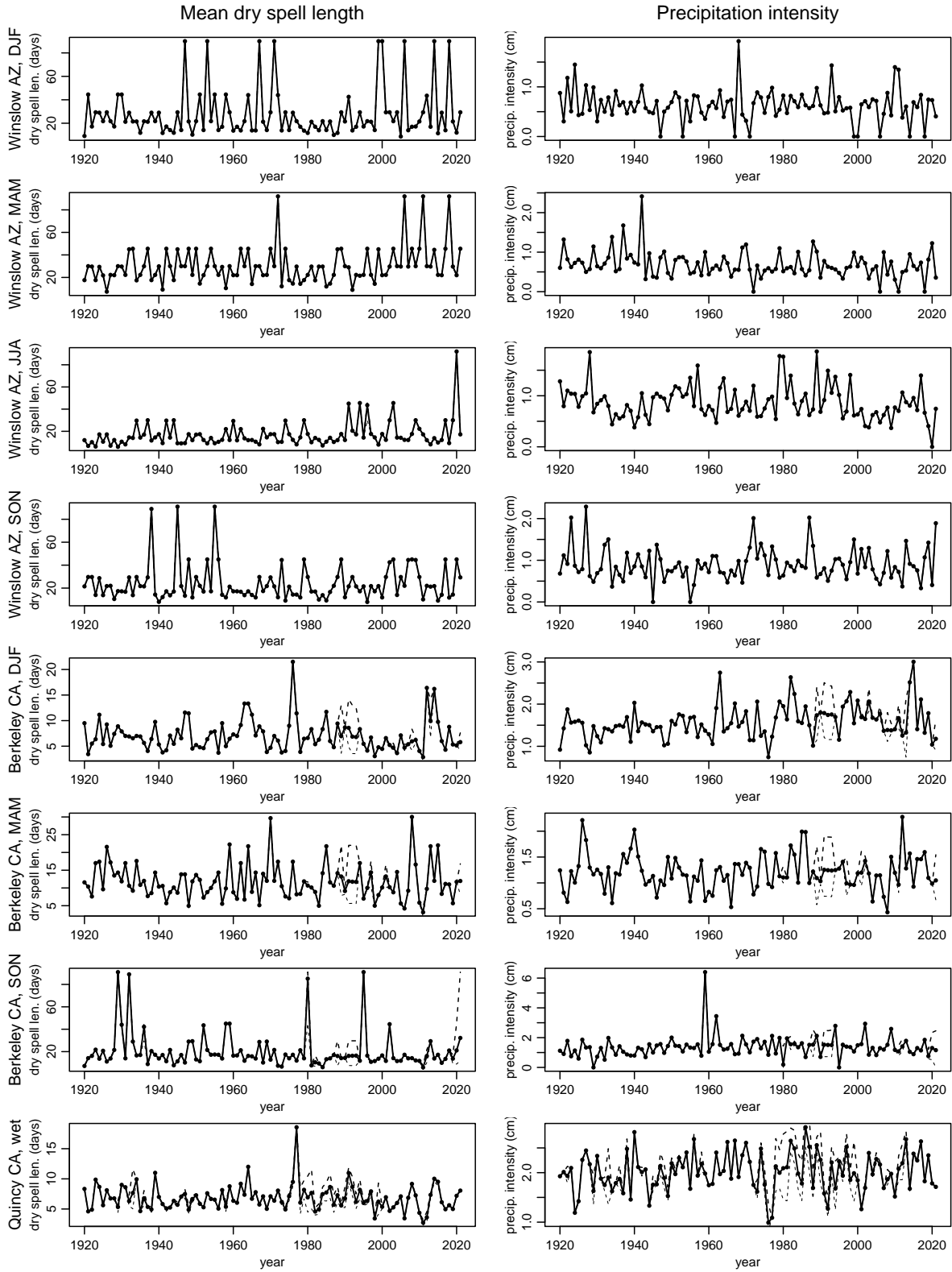


Figure 3: Mean dry spell length (left column) and precipitation intensity (right column) by year for the eight location-season pairs. For years with any missing values, the dry spell length and intensity are the mean over the posterior imputations, with 5% and 95% bounds shown in dashed lines.

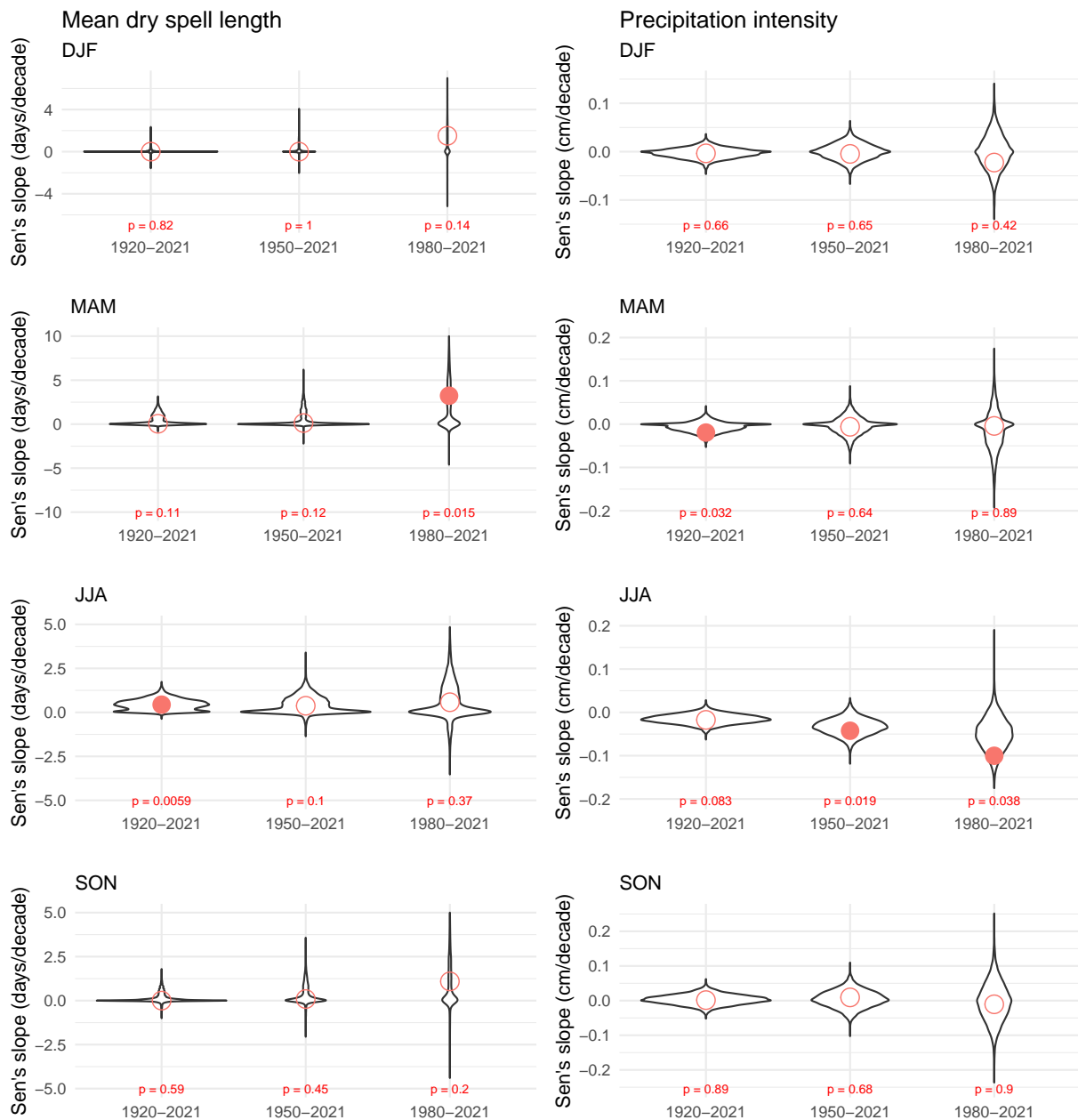


Figure 4: Sen's slope estimates (scaled to be on a per-decade basis) for four seasons (rows: DJF, MAM, JJA, SON) for Winslow based on imputation (red circles; filled circles for estimates with p-values less than 0.05) and the Bayesian posterior (violin plots) for the mean dry spell length (left) and precipitation intensity (right), with p-values for the imputation-based frequentist analysis reported in text in the figure. For the dry spell length (left), the violin plots reflect spikes at zero caused by the spell length being discrete and Sen's slope being the median of pairwise scaled differences between the spell length in different years, with differences of zero being common.

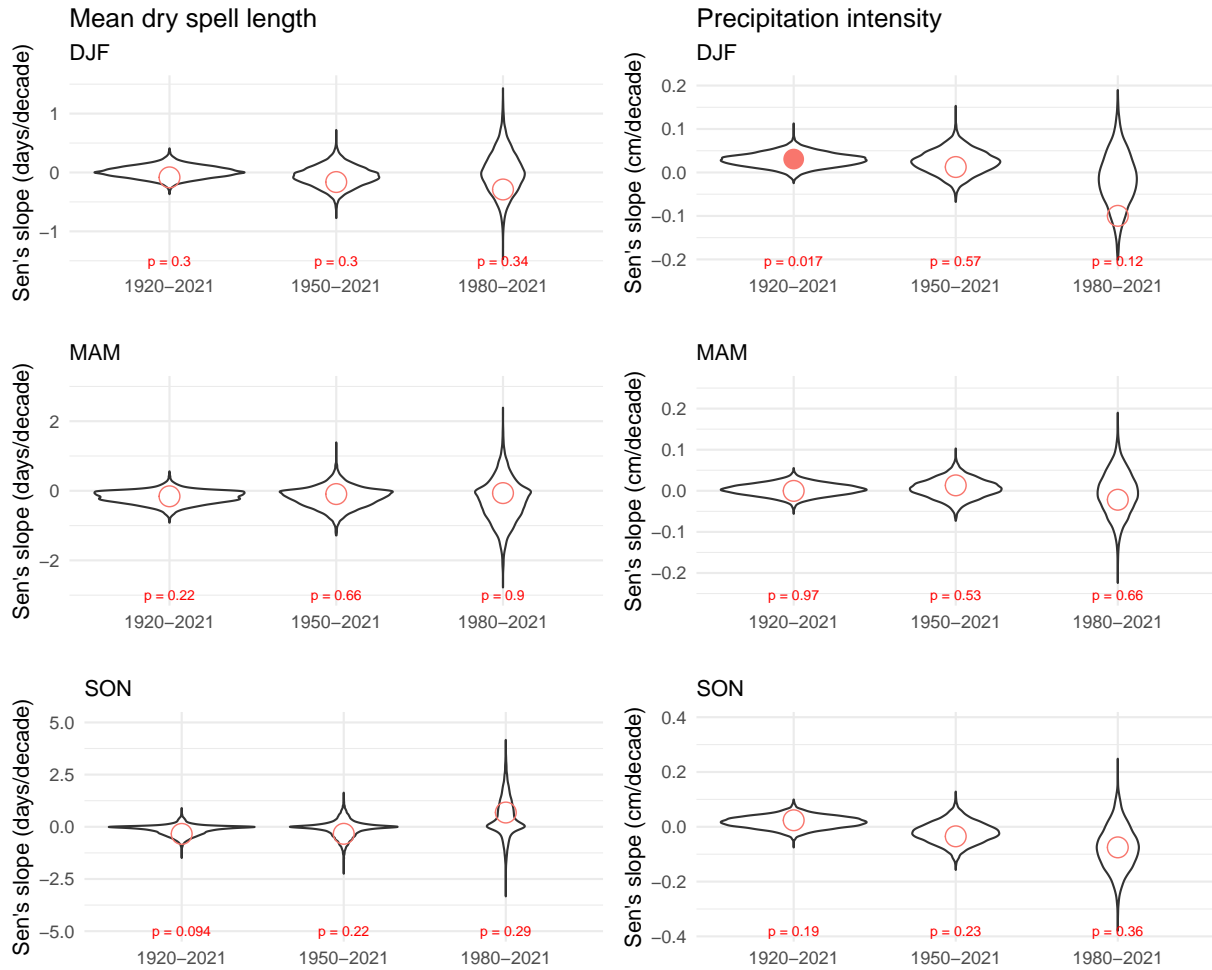


Figure 5: Sen's slope estimates (scaled to be on a per-decade basis) for three seasons (rows: DJF, MAM, SON) for Berkeley based on imputation (red circles; filled circles for estimates with p-values less than 0.05) and the Bayesian posterior (violin plots) for the mean dry spell length (left) and precipitation intensity (right), with p-values for the imputation-based frequentist analysis reported in text in the figure. For the dry spell length (left), the violin plots reflect spikes at zero caused by the spell length being discrete and Sen's slope being the median of pairwise scaled differences between the spell length in different years, with differences of zero being common.

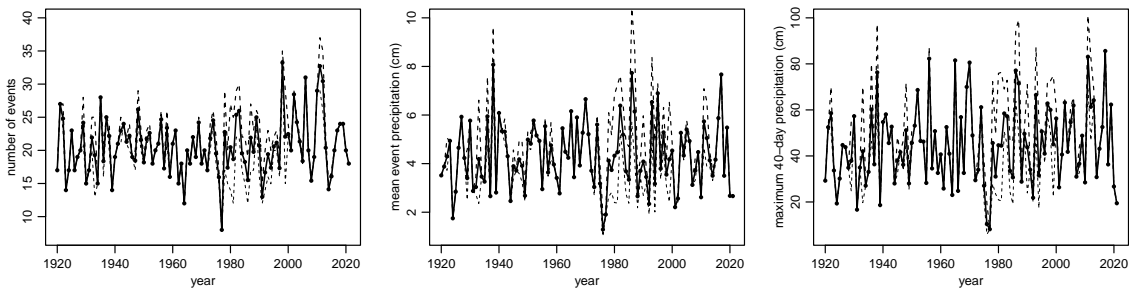


Figure 6: Number of wet spells (left), mean wet spell precipitation (cm) (middle) and maximum 40-day precipitation (cm) (right) by year for Quincy, California. For years with any missing values, the point values are the mean over the posterior imputations, with 5% and 95% bounds shown in dashed lines.

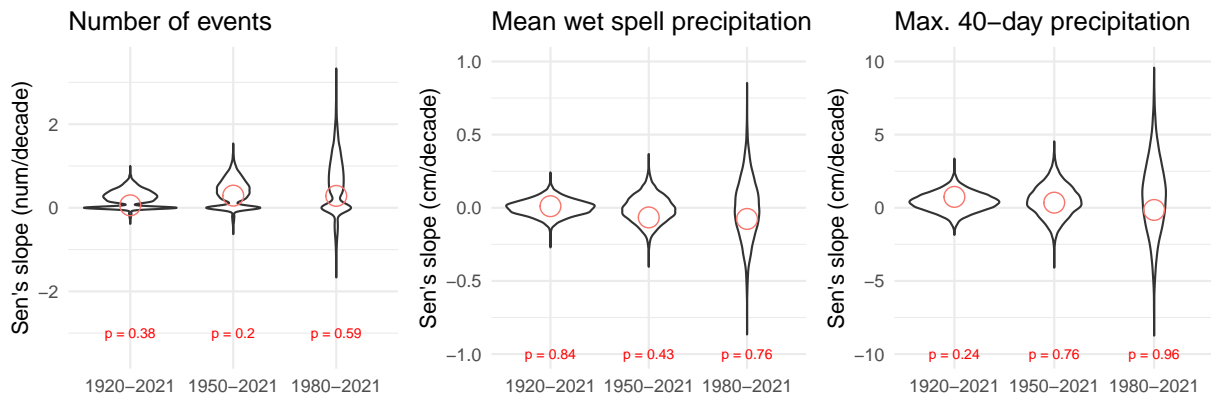


Figure 7: Sen's slope estimates (scaled to be on a per-decade basis) based on imputation (circles) and the Bayesian posterior (violin plots) for the number of precipitation events (left), mean precipitation per event (center) and maximum 40-day precipitation in a season (right), with p-values for the imputation-based frequentist analysis reported in text in the figure. For the number of events (left), the violin plots reflect spikes at zero caused by the number of events being discrete and Sen's slope being the median of pairwise scaled differences between the number of events in different years, with differences of zero being common.

framework. As such, it is suitable for analyzing single time series, which has strengths and limitations. By focusing on a single time series, we have more confidence in the ability of the model to characterize the underlying precipitation dynamics than a more complicated spatio-temporal model, and the method can be used in locations without a network of stations. But it leaves aside the possibility of bringing in additional information that might increase the signal-to-noise ratio, including external information such as radar or satellite data or even other weather variables likely available from the location of interest.

We have used the approach to make inference in two ways. The first is to use the model as an imputation model and then use classical statistical methods to do inference, adjusting for the imputation uncertainty. The second is to use the model within a fully Bayesian framework, doing inference based on the posterior predictive distribution. The latter of course relies more heavily on the statistical model sufficiently capturing the feature of the time series, but it has the benefit of fully Bayesian joint inference for any quantities of interest. The former likely has limited dependence on the model, particularly when missing data are infrequent, while still avoiding the difficulties that missing data pose, both in terms of potential bias from missingness (in particular missing at random mechanisms with respect to year and day of year) and in terms of quantities that cannot be reliably calculated in the face of missing data (such as dry spell lengths).

In our case studies, we find mixed evidence for trends in precipitation patterns based on individual stations, with most of the location-season pairs showing little evidence of trend. This is perhaps not surprising given the high entropy of precipitation. In future work, we will apply the model to large sets of station data (see Zhang et al., 2021 for such an approach). Unlike other such analyses, we will not be as limited by missing data and by the need to determine criteria for removing years of data or making assumptions about the missing values. However, this future work will still suffer from lack of a coherent joint approach to uncertainty in a spatial context. This is a long-standing shortcoming of spatio-temporal analyses. While there is statistical literature on spatial multiple testing (e.g., Sun et al., 2015; Risser et al., 2019), there is not a well-developed general methodology for doing so with spatially-correlated p-values, and Bayesian approaches rely heavily on the statistical model being fit for purpose, a particularly strong assumption in real world spatial settings with complicated spatial nonstationarity. Furthermore, for the questions of interest, it's not clear how much additional information is provided by nearby locations given the spatial extent of weather phenomena. For example, it's not clear that an analysis of a region of California encompassing Berkeley would give substantially more informative results about potential effects of blocking and precipitation variability given that the same weather events affect large spatial areas (particularly where large-scale frontal systems are concerned).

One potential approach that retains the benefit of some simplicity but allows use of multiple locations would be a joint imputation model that seeks to impute missing data for all stations within a spatial region. (Using the methodology presented here, doing imputation individually at multiple stations is not appropriate as the imputed values at a given time will be imputed independently and not reflect the true spatial structure.) Of course such a joint imputation model will rely on the quality of the underlying statistical model with respect to the spatial structure of precipitation. Again, however, by focusing on imputation, one can hope to limit the influence of the model, while still allowing for borrowing of strength spatially without as much concern that the patterns of missingness in space and time may bias results.

Acknowledgments

This research was supported by the Director, Office of Science, Office of Biological and Environmental Research of the U.S. Department of Energy under Contract No. DE-AC02-05CH11231. I thank my CASCADE colleagues for suggestions, in particular Travis O'Brien, Mark Risser, and Michael Wehner.

This document was prepared as an account of work sponsored by the U.S. government. While this document is believed to contain correct information, neither the U.S. government nor any agency thereof, nor the Regents of the University of California, nor any of their employees, makes any warranty, express or implied, or assumes any legal responsibility for the accuracy, completeness, or usefulness of any information, apparatus, product, or process disclosed, or represents that its use would not infringe privately owned rights. Reference herein to any specific commercial product, process, or service by its trade name, trademark, manufacturer, or otherwise, does not necessarily constitute or imply its endorsement, recommendation, or favoring by the U.S. government or any agency thereof, or the Regents of the University of California. The views and opinions of authors expressed herein do not necessarily state or reflect those of the U.S. government or any agency thereof or the Regents of the University of California.

References

- Ailliot, P., D. Allard, V. Monbet, and P. Naveau (2015). Stochastic weather generators: an overview of weather type models. *Journal de la Société Française de Statistique* 156(1), 101–113.
- Chandler, R., V. Isham, P. Northrop, H. Wheeler, C. Onof, and N. Leith (2014). Uncertainty in rainfall inputs. In *Applied Uncertainty Analysis for Flood Risk Management*, pp. 101–152. Imperial College Press.
- Chandler, R. E. and H. S. Wheeler (2002). Analysis of rainfall variability using generalized linear models: a case study from the west of Ireland. *Water Resources Research* 38(10), 1–11.
- de Valpine, P., D. Turek, C. J. Paciorek, C. Anderson-Bergman, D. T. Lang, and R. Bodik (2017). Programming with models: writing statistical algorithms for general model structures with NIMBLE. *Journal of Computational and Graphical Statistics* 26(2), 403–413.
- Easterling, D., K. Kunkel, J. Arnold, T. Knutson, A. LeGrande, L. Leung, R. Vose, D. Waliser, and M. Wehner (2017). Precipitation change in the United States. In D. Wuebbles, D. Fahey, K. Hibbard, D. Dokken, B. Stewart, and T. Maycock (Eds.), *Climate Science Special Report: Fourth National Climate Assessment, Volume I*, Chapter 7, pp. 207–230. Washington, DC: U.S. Global Change Research Program.
- Furrer, E. M. and R. W. Katz (2008). Improving the simulation of extreme precipitation events by stochastic weather generators. *Water Resources Research* 44(12), W12439.
- Helsel, D. R. and L. M. Frans (2006). Regional Kendall test for trend. *Environmental Science & Technology* 40(13), 4066–4073.

- Holsclaw, T., A. M. Greene, A. W. Robertson, and P. Smyth (2017). Bayesian nonhomogeneous Markov models via Pólya-gamma data augmentation with applications to rainfall modeling. *The Annals of Applied Statistics* 11(1), 393–426.
- Hug, J. E. and C. J. Paciorek (2021). A numerically stable online implementation and exploration of WAIC through variations of the predictive density, using NIMBLE. arXiv preprint 2106.13359.
- Huxman, T. E., K. A. Snyder, D. Tissue, A. J. Leffler, K. Ogle, W. T. Pockman, D. R. Sandquist, D. L. Potts, and S. Schwinning (2004). Precipitation pulses and carbon fluxes in semiarid and arid ecosystems. *Oecologia* 141(2), 254–268.
- IPCC (2021). *Climate Change 2021: The Physical Science Basis. Contribution of Working Group I to the Sixth Assessment Report of the Intergovernmental Panel on Climate Change*. Cambridge University Press.
- IPCC (2022). *Climate Change 2022: Impacts, Adaptation, and Vulnerability. Contribution of Working Group II to the Sixth Assessment Report of the Intergovernmental Panel on Climate Change*. Cambridge University Press.
- Jefferys, W. H. and J. O. Berger (1992). Ockham’s razor and Bayesian analysis. *American Scientist* 80(1), 64–72.
- Kasler and Hecht (2017). As emergency spillway flows, state says repairs to crippled Oroville dam could run \$200 million. Sacramento Bee, 2017-02-12.
- Lall, U., T. Johnson, P. Colohan, A. Aghakouchak, C. Brown, G. McCabe, R. Pulwarty, and A. Sankarasubramanian (2017). Water. In D. Reidmiller, C. Avery, D. Easterling, K. Kunkel, K. Lewis, T. Maycock, and B. Stewart (Eds.), *Impacts, Risks, and Adaptation in the United States: Fourth National Climate Assessment, Volume II*, Chapter 3, pp. 145–173. Washington, DC: U.S. Global Change Research Program.
- MacKay, D. J. (2003). *Information Theory, Inference and Learning Algorithms*. Cambridge University Press.
- Martinez-Villalobos, C. and J. D. Neelin (2019). Why do precipitation intensities tend to follow gamma distributions? *Journal of the Atmospheric Sciences* 76(11), 3611–3631.
- Menne, M. J., I. Durre, B. Korzeniewski, S. McNeill, K. Thomas, X. Yin, S. Anthony, R. Ray, R. S. Vose, B. E. Gleason, and T. G. Houston (2012). Global historical climatology network - daily (GHCN-Daily), version 3.
- National Academies of Sciences, Engineering, and Medicine (2016). *Attribution of Extreme Weather Events in the Context of Climate Change*. The National Academies Press.
- Naveau, P., R. Huser, P. Ribereau, and A. Hannart (2016). Modeling jointly low, moderate, and heavy rainfall intensities without a threshold selection. *Water Resources Research* 52(4), 2753–2769.

- NIMBLE Development Team (2022, February). NIMBLE: MCMC, Particle Filtering, and Programmable Hierarchical Modeling, Version 0.12.2.
- Risser, M. D., C. J. Paciorek, T. A. O'Brien, M. F. Wehner, and W. D. Collins (2019). Detected changes in precipitation extremes at their native scales derived from in situ measurements. *Journal of Climate* 32(23), 8087–8109.
- Risser, M. D., C. J. Paciorek, and D. A. Stone (2019). Spatially dependent multiple testing under model misspecification, with application to detection of anthropogenic influence on extreme climate events. *Journal of the American Statistical Association* 114(525), 61–78.
- Sen, P. K. (1968). Estimates of the regression coefficient based on Kendall's tau. *Journal of the American Statistical Association* 63(324), 1379–1389.
- Stan Development Team (2020). RStan: the R interface to Stan. R package version 2.21.2.
- Stoner, O. and T. Economou (2020). An advanced hidden Markov model for hourly rainfall time series. *Computational Statistics & Data Analysis* 152, 107045.
- Sun, W., B. J. Reich, T. T. Cai, M. Guindani, and A. Schwartzman (2015). False discovery control in large-scale spatial multiple testing. *Journal of the Royal Statistical Society, Series B (Statistical Methodology)* 77(1), 59.
- Swain, D. L., B. Langenbrunner, J. D. Neelin, and A. Hall (2018). Increasing precipitation volatility in twenty-first-century California. *Nature Climate Change* 8(5), 427–433.
- Vehtari, A., A. Gelman, and J. Gabry (2017). Practical Bayesian model evaluation using leave-one-out cross-validation and WAIC. *Statistics and Computing* 27(5), 1413–1432.
- Vehtari, A., A. Gelman, D. Simpson, B. Carpenter, and P.-C. Bürkner (2021). Rank-normalization, folding, and localization: an improved \hat{f} for assessing convergence of MCMC (with discussion). *Bayesian Analysis* 16(2), 667–718.
- Wang, S.-Y., L. Hippias, R. R. Gillies, and J.-H. Yoon (2014). Probable causes of the abnormal ridge accompanying the 2013–2014 California drought: ENSO precursor and anthropogenic warming footprint. *Geophysical Research Letters* 41(9), 3220–3226.
- Wang, S.-Y. S., J.-H. Yoon, E. Becker, and R. Gillies (2017). California from drought to deluge. *Nature Climate Change* 7(7), 465–468.
- Westra, S., L. V. Alexander, and F. W. Zwiers (2013). Global increasing trends in annual maximum daily precipitation. *Journal of Climate* 26(11), 3904–3918.
- Wilks, D. S. and R. L. Wilby (1999). The weather generation game: a review of stochastic weather models. *Progress in Physical Geography* 23(3), 329–357.
- Wood, R. R., F. Lehner, A. G. Pendergrass, and S. Schlunegger (2021). Changes in precipitation variability across time scales in multiple global climate model large ensembles. *Environmental Research Letters* 16(8), 084022.

- Wood, S. N. (2017). *Generalized Additive Models: An Introduction with R* (2 ed.). Chapman and Hall/CRC.
- Woody, S., C. M. Carvalho, and J. S. Murray (2021). Model interpretation through lower-dimensional posterior summarization. *Journal of Computational and Graphical Statistics* 30(1), 144–161.
- Yang, C., R. Chandler, V. Isham, and H. Wheeler (2005). Spatial-temporal rainfall simulation using generalized linear models. *Water Resources Research* 41(11), W11415.
- Zhang, F., J. A. Biederman, M. P. Dannenberg, D. Yan, S. C. Reed, and W. K. Smith (2021). Five decades of observed daily precipitation reveal longer and more variable drought events across much of the western United States. *Geophysical Research Letters* 48(7), e2020GL092293.
- Zhang, W., K. Furtado, P. Wu, T. Zhou, R. Chadwick, C. Marzin, J. Rostron, and D. Sexton (2021). Increasing precipitation variability on daily-to-multiyear time scales in a warmer world. *Science Advances* 7(31), eabf8021.
- Zhang, X., F. W. Zwiers, G. C. Hegerl, F. H. Lambert, N. P. Gillett, S. Solomon, P. A. Stott, and T. Nozawa (2007). Detection of human influence on twentieth-century precipitation trends. *Nature* 448(7152), 461–465.

Supplemental figures and tables

Table 3: Median (99th percentile) \hat{R} MCMC diagnostic across 102 yearly values (or ~90 day of season values) for various quantities for the eight location-seasons.

	yearly prob. rain > 3 mm	yearly prob. rain > 10 mm	yearly prob. rain > 20 mm	day of year prob. rain > 3 mm	day of year prob. rain > 10 mm	day of year prob. rain > 20 mm	yearly prob. dry to dry	yearly prob. wet to dry	yearly mean dry spell length	yearly precipi- tation intensity
Winslow AZ, DJF	1.001 (1.004)	1.001 (1.002)	1.000 (1.002)	1.001 (1.004)	1.000 (1.002)	1.000 (1.002)	1.001 (1.004)	1.000 (1.003)	1.001 (1.004)	1.000 (1.002)
Winslow AZ, MAM	1.000 (1.001)	1.000 (1.002)	1.000 (1.001)	1.000 (1.001)	1.000 (1.002)	1.000 (1.001)	1.000 (1.001)	1.000 (1.001)	1.000 (1.001)	1.000 (1.001)
Winslow AZ, JJA	1.001 (1.014)	1.001 (1.009)	1.001 (1.010)	1.002 (1.008)	1.001 (1.022)	1.001 (1.014)	1.002 (1.011)	1.001 (1.007)	1.002 (1.011)	1.001 (1.009)
Winslow AZ, SON	1.001 (1.002)	1.000 (1.001)	1.000 (1.001)	1.001 (1.004)	1.000 (1.002)	1.000 (1.001)	1.000 (1.002)	1.001 (1.002)	1.000 (1.002)	1.000 (1.001)
Berkeley CA, DJF	1.001 (1.004)	1.001 (1.011)	1.001 (1.006)	1.002 (1.012)	1.001 (1.015)	1.001 (1.011)	1.001 (1.008)	1.001 (1.014)	1.001 (1.007)	1.001 (1.003)
Berkeley CA, MAM	1.001 (1.003)	1.001 (1.004)	1.001 (1.002)	1.002 (1.006)	1.001 (1.006)	1.001 (1.004)	1.001 (1.004)	1.001 (1.002)	1.001 (1.004)	1.001 (1.002)
Berkeley CA, SON	1.000 (1.001)	1.000 (1.001)	1.000 (1.002)	1.001 (1.008)	1.000 (1.005)	1.000 (1.005)	1.000 (1.001)	1.000 (1.002)	1.000 (1.002)	1.000 (1.001)
Quincy CA, wet (Nov-Apr)	1.000 (1.002)	1.000 (1.002)	1.000 (1.002)	1.000 (1.003)	1.000 (1.003)	1.000 (1.003)	1.000 (1.002)	1.000 (1.002)	1.000 (1.001)	1.000 (1.002)

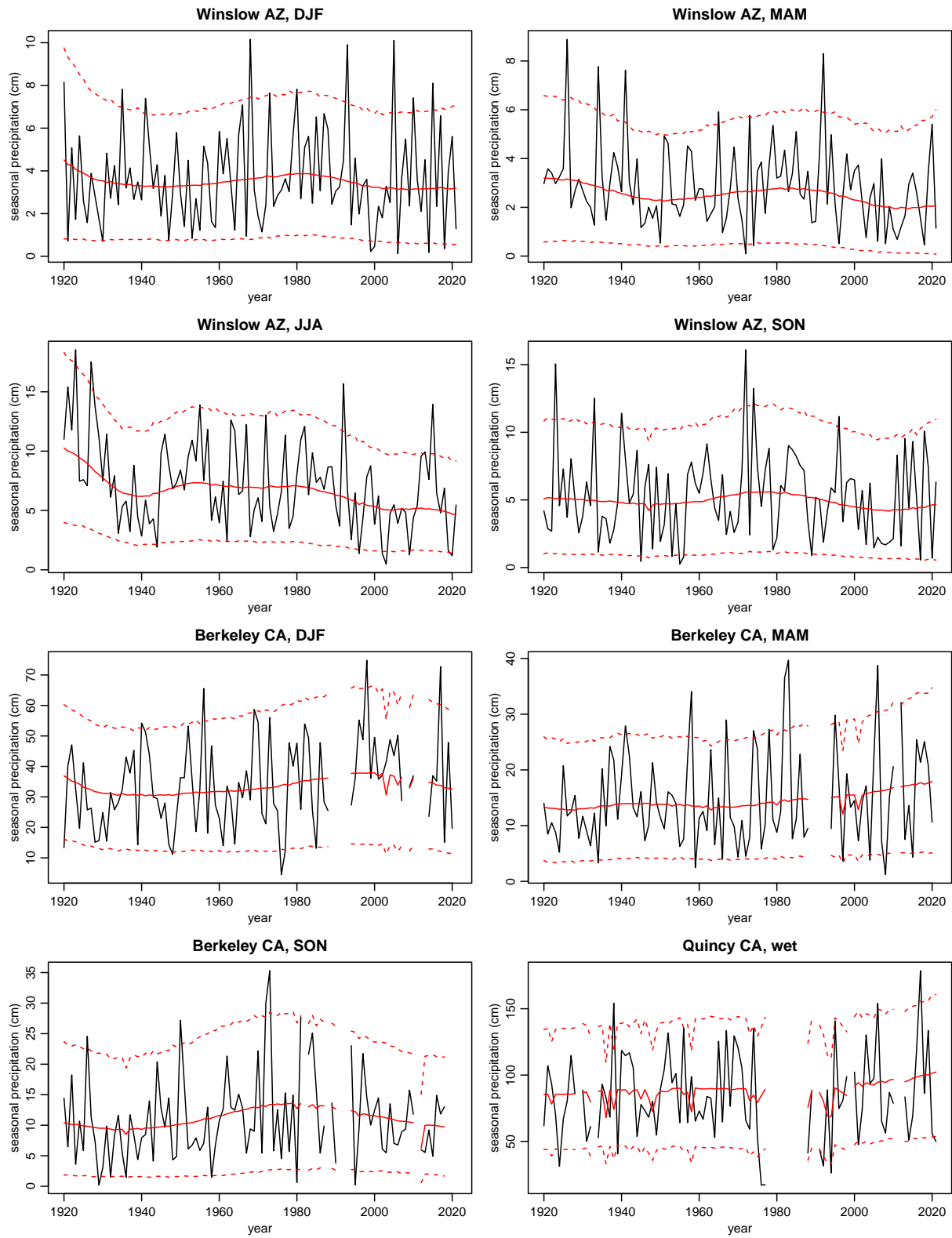


Figure 8: Observed (black) versus simulated (red) total seasonal precipitation by year for the eight location-season pairs, omitting years in which more than 25% of observations were missing. Simulated values are the mean over the simulations, with 90% predictive uncertainty bands.

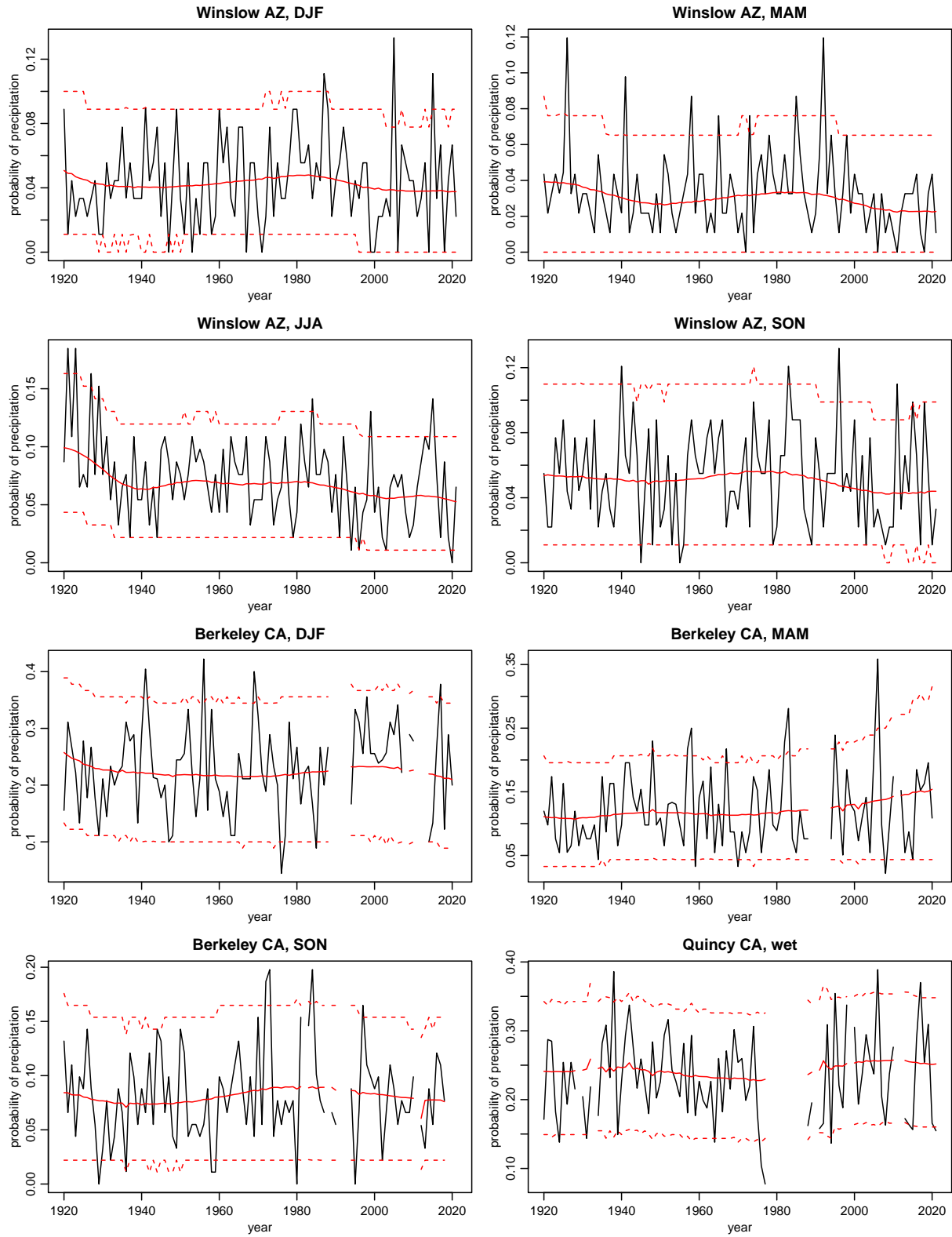


Figure 9: Observed versus simulated probability of non-negligible precipitation (greater than three mm) by year for the eight location-season pairs, omitting years in which more than 25% of observations were missing. Simulated values are the mean over the simulations, with 90% predictive uncertainty bands.

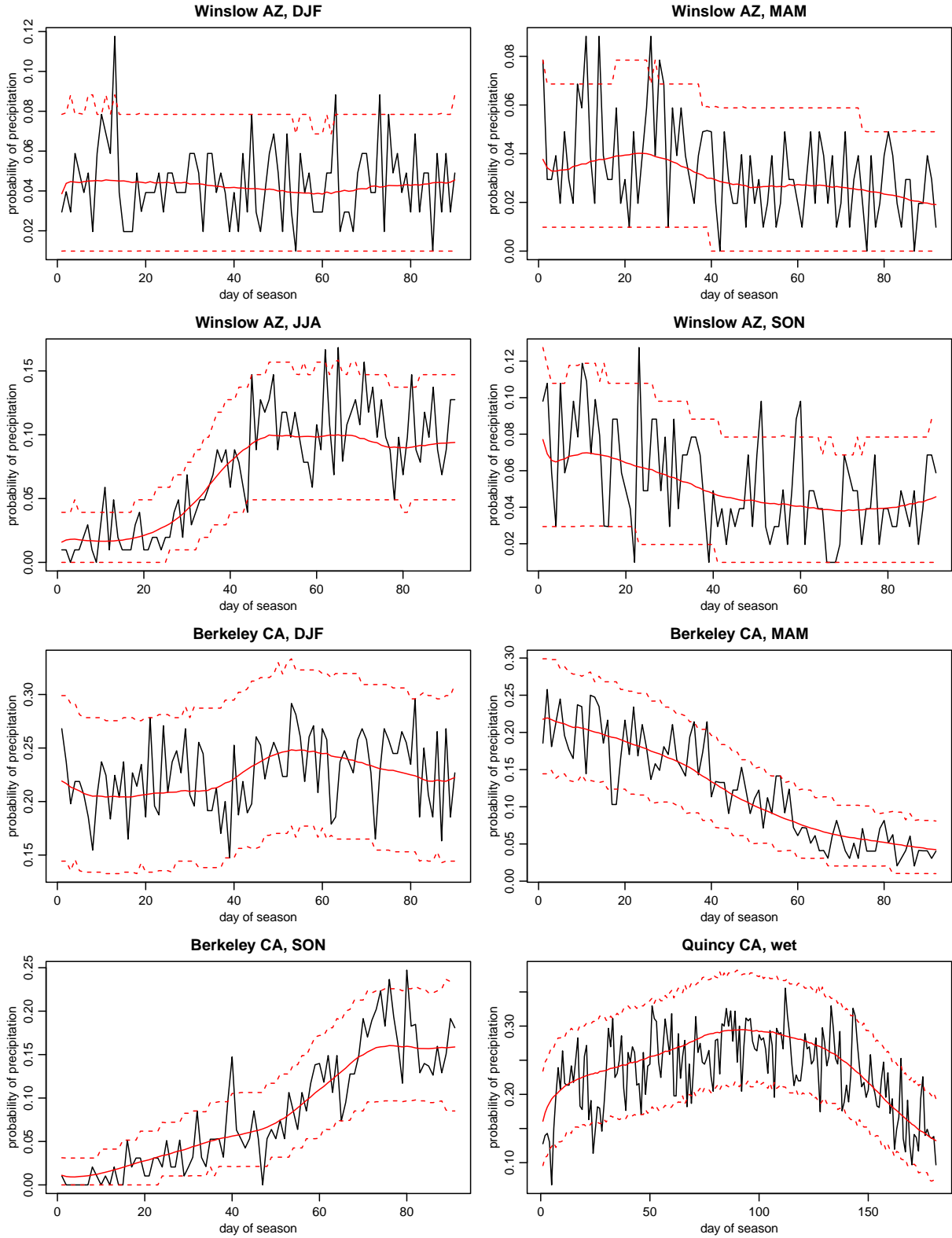


Figure 10: Observed versus simulated probability of non-negligible precipitation (greater than three mm) within season (by day of season) for the eight location-season pairs, omitting days of the year in which more than 25% of observations were missing. Simulated values are the mean over the simulations, with 90% predictive uncertainty bands.

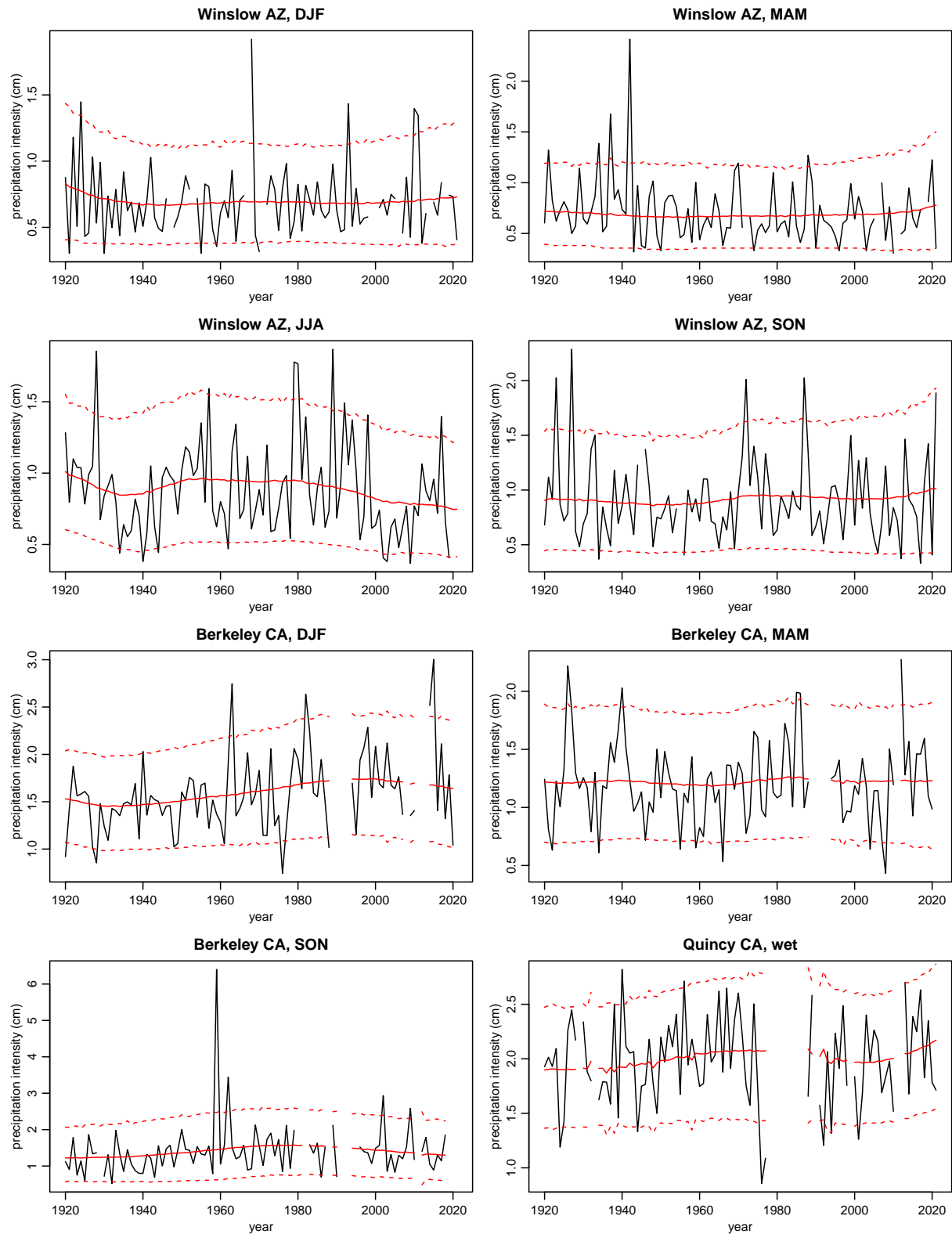


Figure 11: Observed versus simulated precipitation intensity (mean of precipitation over days with non-negligible precipitation (greater than three mm)) by year for the eight location-season pairs, omitting years in which more than 25% of observations were missing (and omitting observed values for years with no days with non-negligible precipitation). Simulated values are the mean over the simulations, with 90% predictive uncertainty bands.

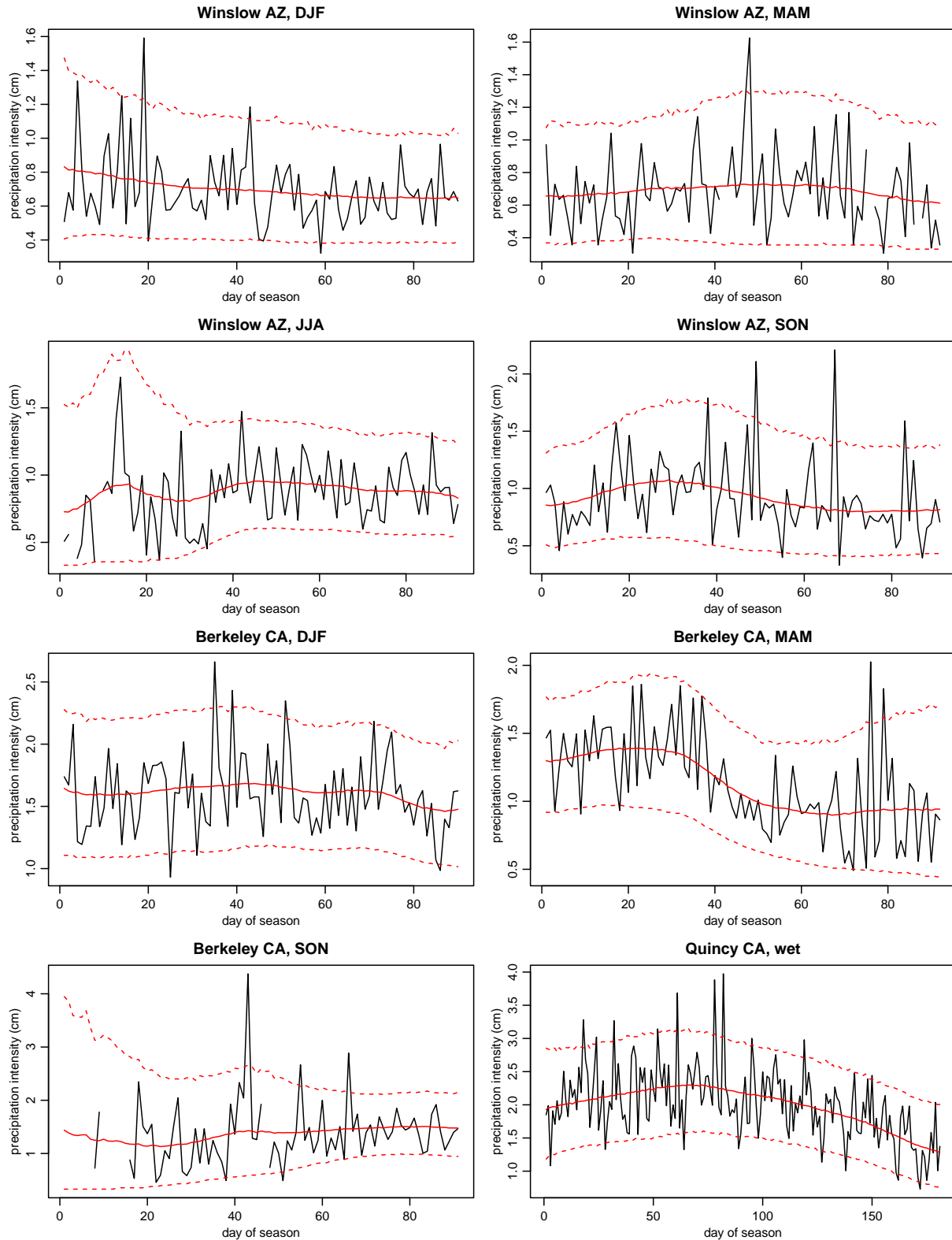


Figure 12: Observed versus simulated precipitation intensity (mean of precipitation over days with non-negligible precipitation (greater than three mm)) within season (by day of season) for the eight location-season pairs, omitting days of the season in which more than 25% of observations were missing (and omitting observed values for days of the year with no days with non-negligible precipitation). Simulated values are the mean over all the simulations, with 90% predictive uncertainty bands.

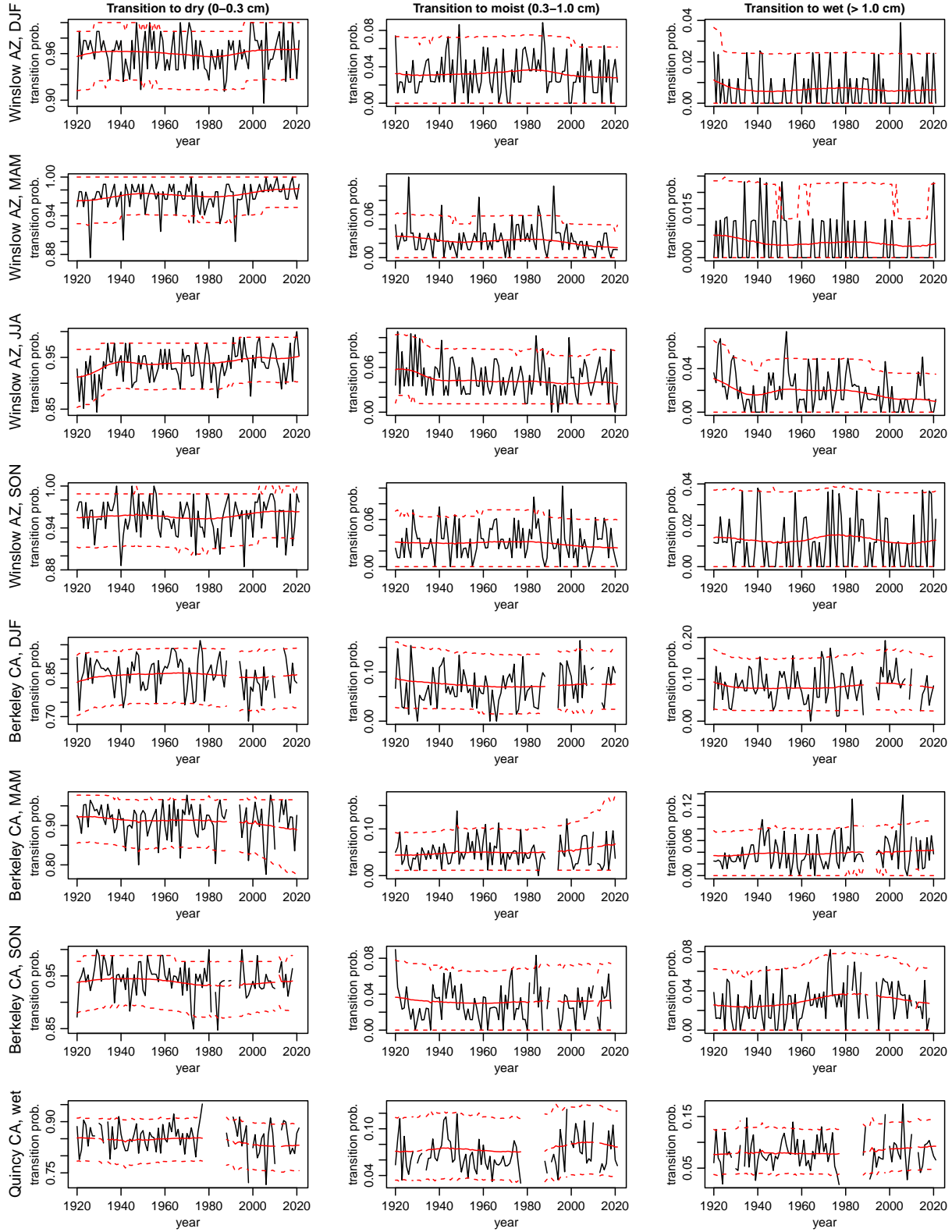


Figure 13: Observed versus simulated probability of dry (0-0.3 cm; first column), moist (0.3-1 cm; second column), or wet (>1 cm; third column) day given the previous day was dry (0-0.3 cm) by year, for the eight location-season pairs (rows). Years in which more than 25% of observations were missing are omitted. Simulated values are the mean over the simulations, with 90% predictive uncertainty bands.

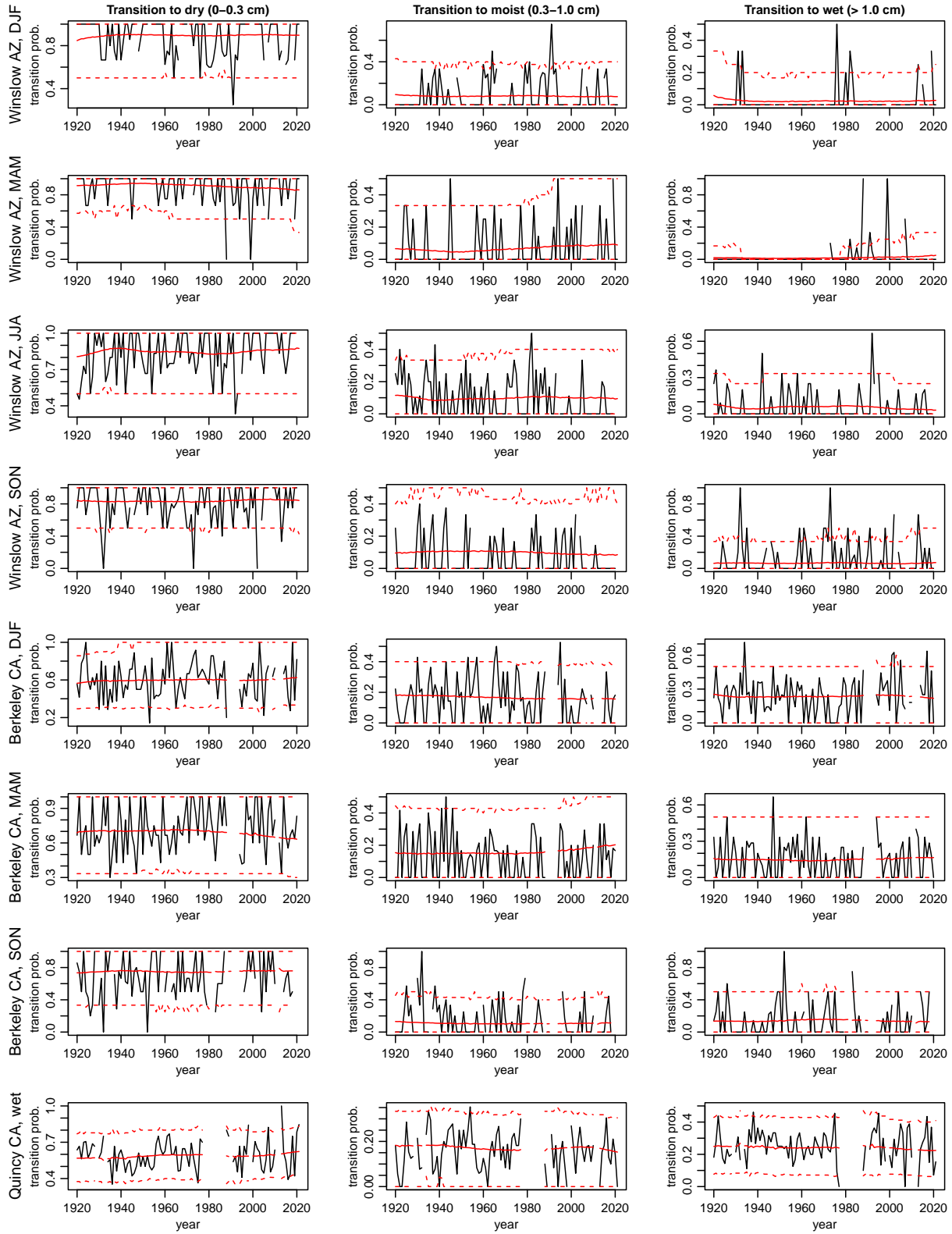


Figure 14: Observed versus simulated probability of dry (0-0.3 cm; first column), moist (0.3-1 cm; second column), or wet (>1 cm; third column) day given the previous day was moist (0.3-1 cm) by year, for the eight location-season pairs (rows). Years in which more than 25% of observations were missing are omitted (as are values for years in which there are no moist days). Simulated values are the mean over the simulations, with 90% predictive uncertainty bands. Missing values can occur when there are no moist days in a year.

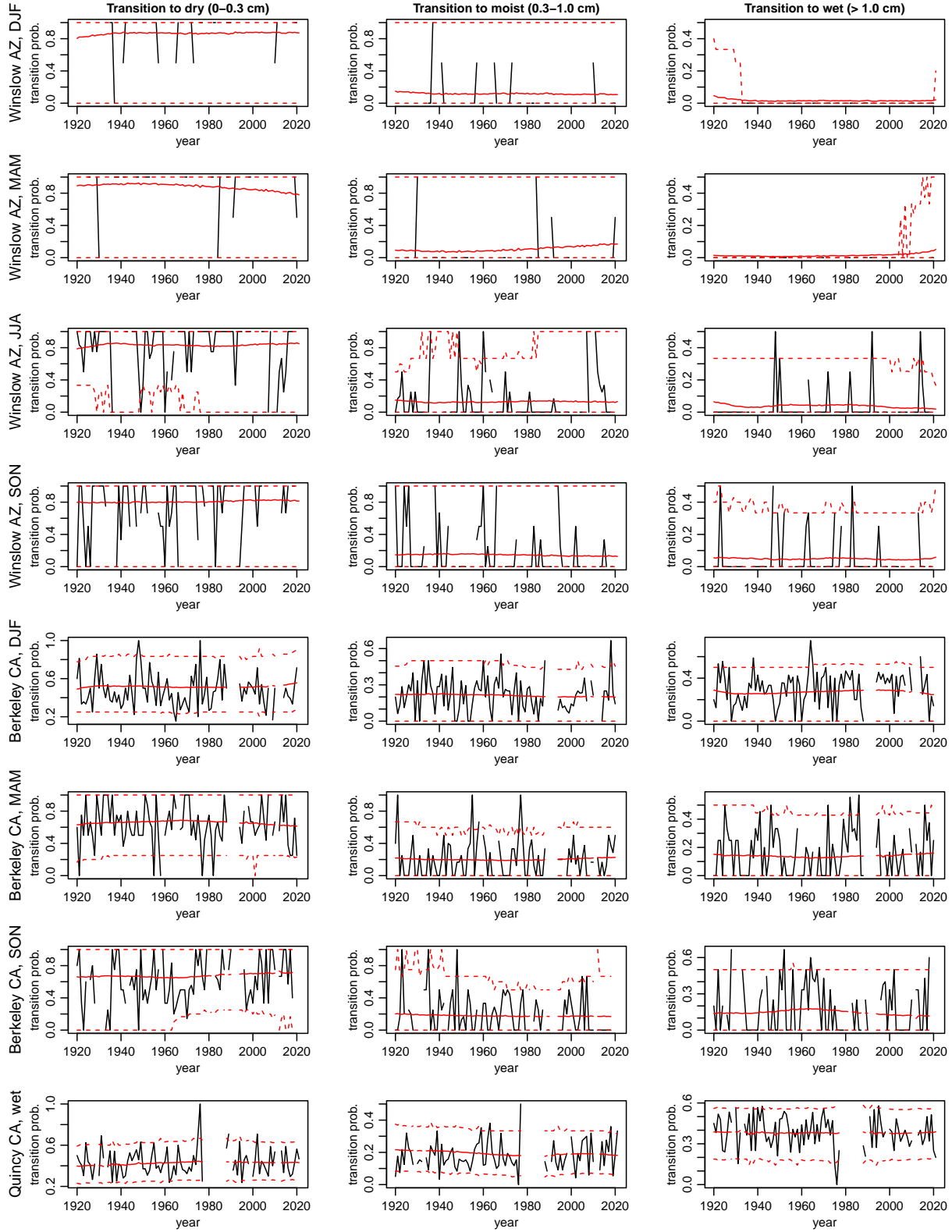


Figure 15: Observed versus simulated probability of dry (0-0.3 cm; first column), moist (0.3-1 cm; second column), or wet (>1 cm; third column) day given the previous day was wet (>1 cm) by year, for the eight location-season pairs (rows). Years in which more than 25% of observations were missing are omitted (as are values for years in which there are no wet days). Simulated values are the mean over the simulations, with 90% predictive uncertainty bands.

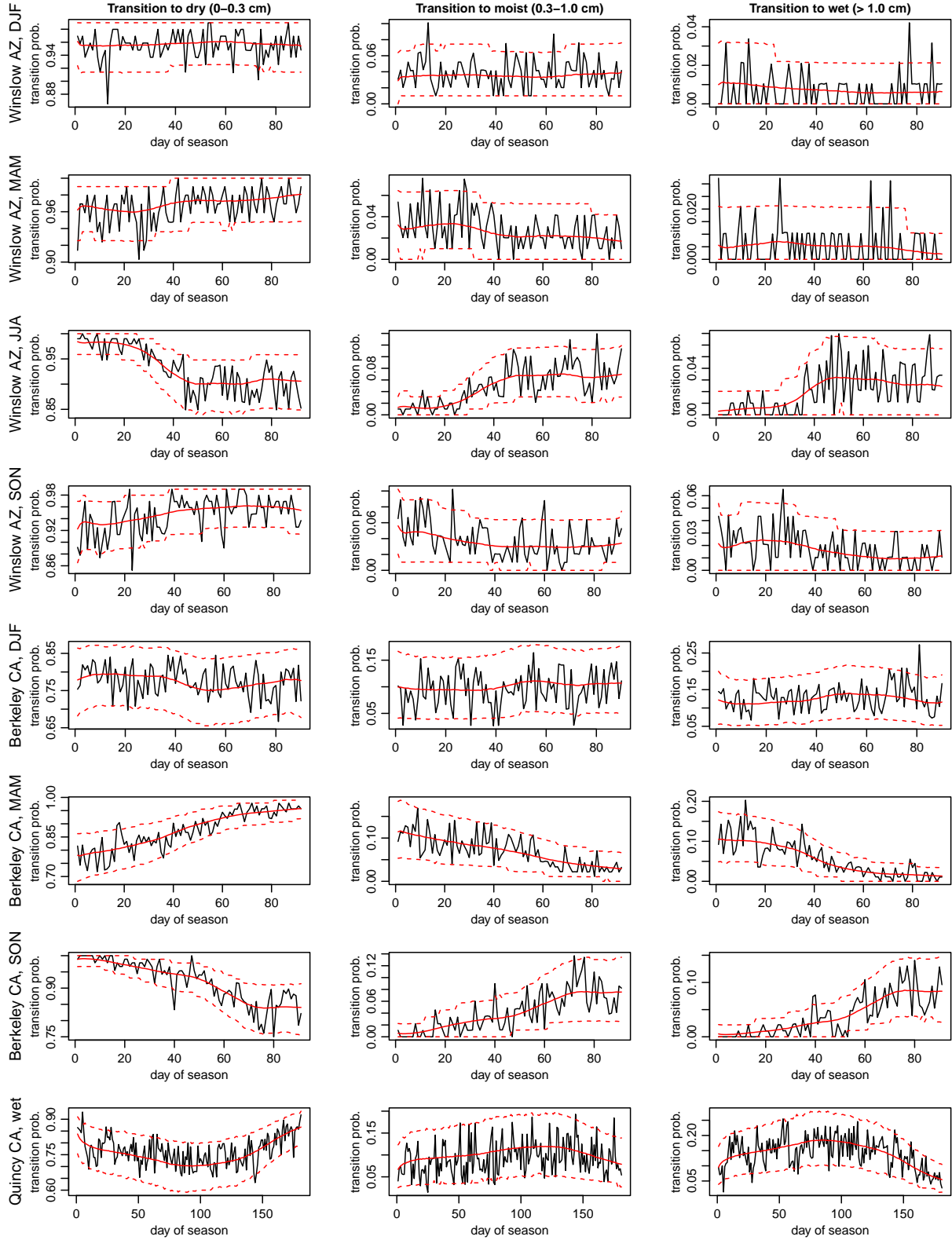


Figure 16: Observed versus simulated probability of dry (0-0.3 cm; first column), moist (0.3-1 cm; second column), or wet (>1 cm; third column) day given the previous day was dry (0-0.3 cm) within season (by day of season), for the eight location-season pairs (rows). Simulated values are the mean over the simulations, with 90% predictive uncertainty bands.

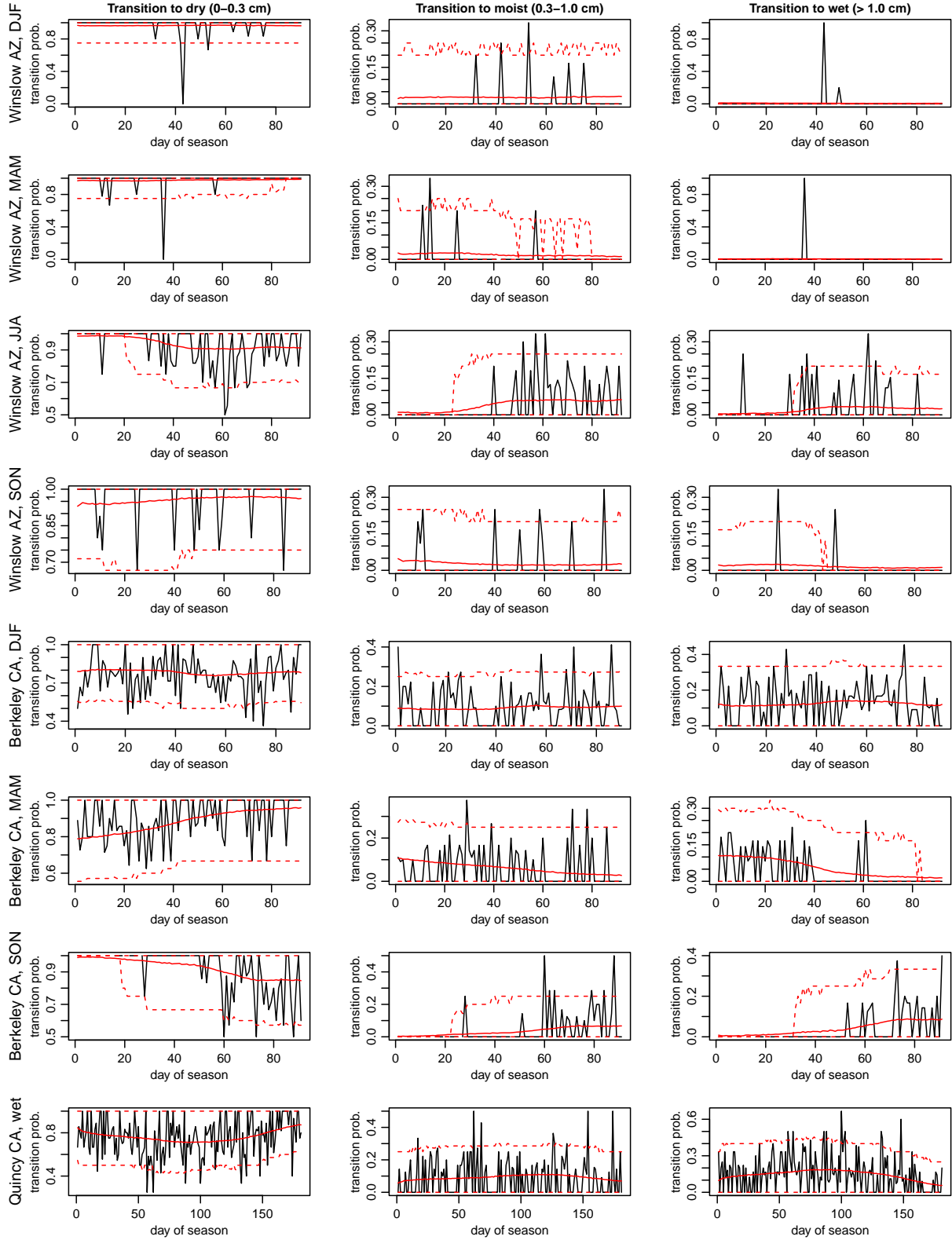


Figure 17: Observed versus simulated probability of dry (0-0.3 cm; first column), moist (0.3-1 cm; second column), or wet (>1 cm; third column) day given the previous day was moist (0.3-1 cm) within season (by day of season), for the eight location-season pairs (rows). Days of season in which more than 25% of observations were missing are omitted (as are values for days of season in which there are no moist days). Simulated values are the mean over the simulations, with 90% predictive uncertainty bands.

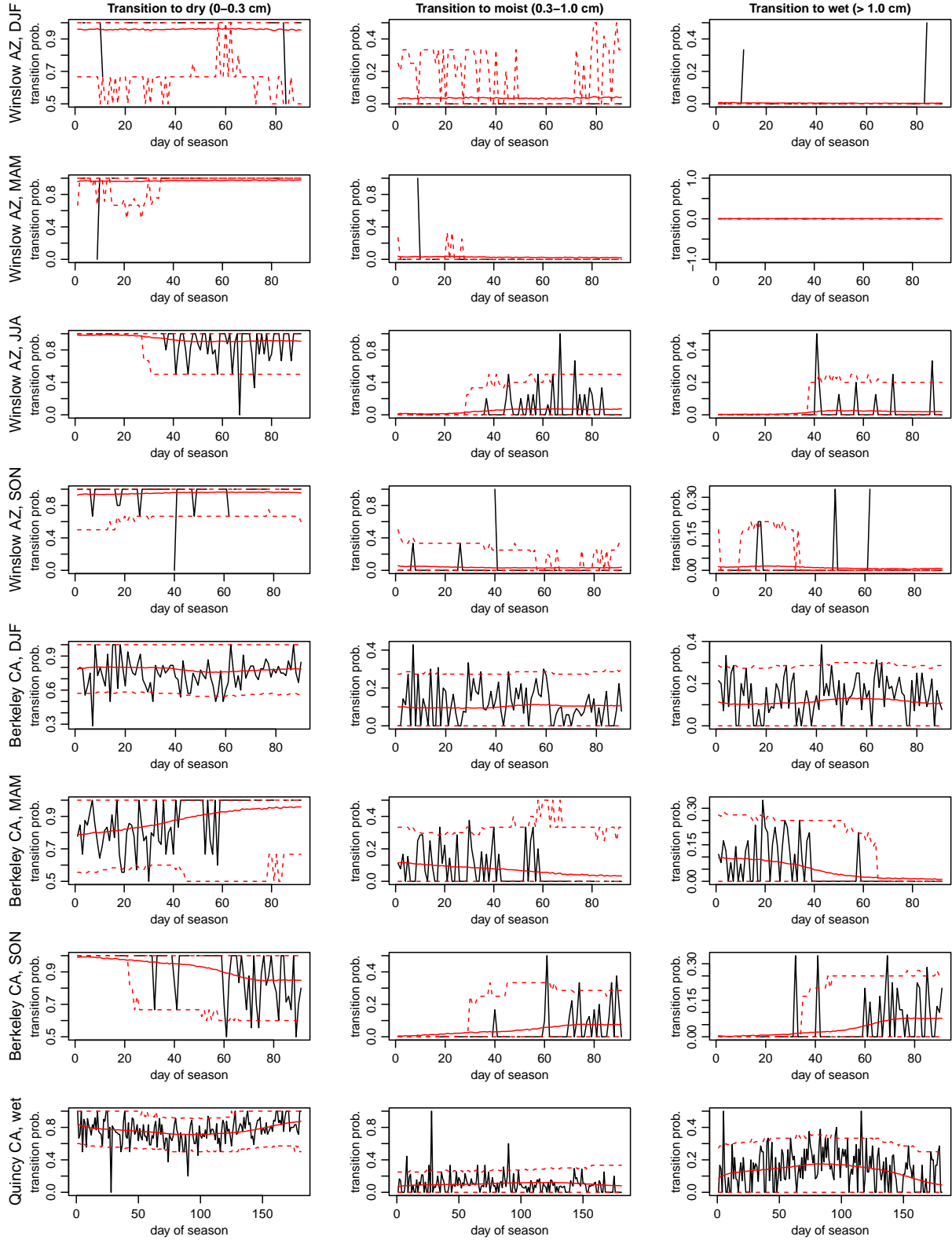


Figure 18: Observed versus simulated probability of dry (0-0.3 cm; first column), moist (0.3-1 cm; second column), or wet (>1 cm; third column) day given the previous day was wet (>1 cm) within season (by day of season), for the eight location-season pairs (rows). Days of season in which more than 25% of observations were missing are omitted (as are values for days of season in which there are no wet days). Simulated values are the mean over the simulations, with 90% predictive uncertainty bands.

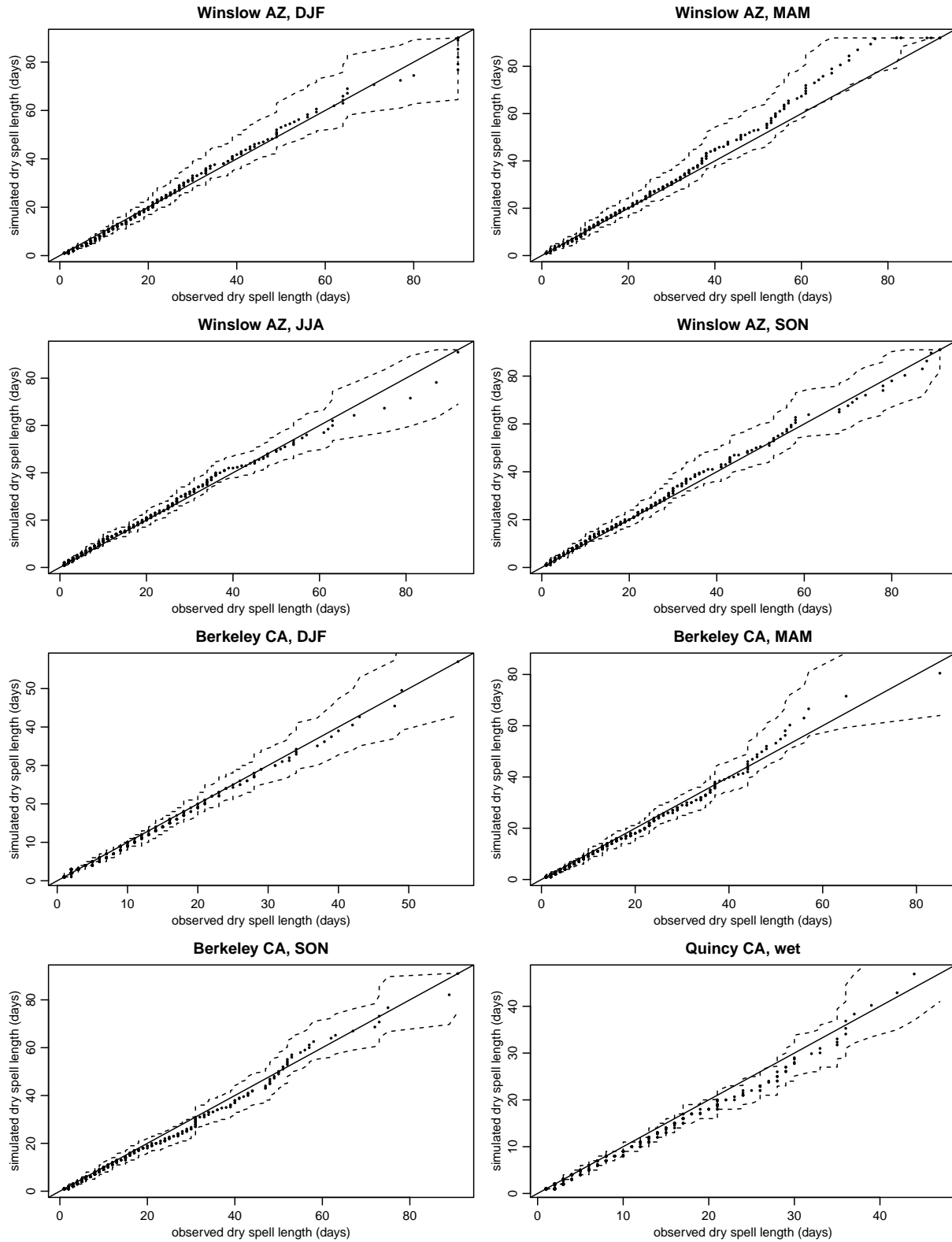


Figure 19: Median and 95% predictive intervals for Q-Q comparisons of the simulated versus observed dry spell lengths for the eight location-season pairs (rows). The median and 95% intervals are taken over Q-Q comparisons of each simulated time series against the observed values. If simulated values are consistent with the observed values, we expect the points (the median values) near the 1:1 line and the intervals to generally cover the 1:1 line.